The influence of multiple groups of biological ice nucleating particles on microphysical properties of mixed-phase clouds observed during MC3E

Sachin Patade[1*], Deepak Waman[1], Akash Deshmukh[1], Ashok Kumar Gupta[2], Arti Jadav[1], Vaughan Phillips[1], Aaron Bansemer[4], Jacob Carlin[3], Alexander Ryzhkov[3],

[1]Department of Physical Geography and Ecosystem Science, Lund University, Lund, Sweden

[2]Department of Earth and Environmental Sciences, Vanderbilt University, Nashville, TN, 37240, USA

[3]Cooperative Institute for Severe and High-Impact Weather Research and Operations, The University of Oklahoma, and NOAA/OAR National Severe Storms Laboratory, Norman, Oklahoma, USA

[4]National Center for Atmospheric Research, Boulder, Colorado, USA

*** Corresponding Author**

Dr. Sachin Patade, Lund University, Sweden

email: sachin.patade@nateko.lu.se

Abstract:

A new empirical parameterization (EP) for multiple groups of primary biological aerosol particles (PBAPs) is implemented in the aerosol-cloud model (AC) to investigate their roles as ice-nucleating particles (INPs). The EP describes the heterogeneous ice nucleation by (1) fungal spores, (2) bacteria, (3) pollen, (4) detritus of plants, animals, and viruses, and (5) algae. Each group includes fragments from the originally emitted particles. A high-resolution simulation of a midlatitude mesoscale squall line by AC is validated against airborne and ground observations.

Sensitivity tests are carried out by varying the initial vertical profiles of the loadings of individual PBAP groups. The resulting changes in warm and ice cloud microphysical parameters are investigated. The changes in warm microphysical parameters including liquid water content, and cloud droplet number concentration are minimal (< 10%). Overall, PBAPs have little effect on ice number concentration (< 6%) in the convective region. In the stratiform region, increasing the initial PBAP loadings by a factor of 1000 resulted in less than 40% change in ice number concentrations. The total ice concentration is mostly controlled by various mechanisms of secondary ice production (SIP). However, when SIP is intentionally shut down in sensitivity tests, increasing the PBAP loading by a factor of 100 has less than a 3% effect on the ice phase. Further sensitivity tests revealed that PBAPs have little effect on surface precipitation as well as on shortwave and longwave flux (< 4%) for 100-fold perturbation in PBAPs.

1. Introduction

In most climate models, the largest source of uncertainty for estimating the total anthropogenic forcing is associated with cloud-aerosol interactions (Pörtner et al., 2022). Atmospheric aerosol particles can act as cloud condensation nuclei (CCN) and a few of them

act as ice-nucleating particles (INPs), thereby influencing the microphysical properties of clouds and, depending on the cloud type (Fan et al. 2010; Chen et al 2019). The treatment of INP in climate models can strongly affect the atmospheric radiation budget (DeMott et al. 2010). Various sources of aerosol particles, including dust/metallic, marine aerosols, anthropogenic carbonaceous emissions, and primary biological aerosol particles (PBAPs), contribute to the observed INPs (Kanji et al. 2017).

A significant amount of global precipitation is associated with the ice phase in cold clouds (Heymsfield and Field 2015; Mülmenstädt et al. 2015, Heymsfield et al. 2020). In particular, mixed-phase clouds are vital for the global climate (Dong and Mace 2003; Zuidema et al. 2005; Matus and L'Ecuyer 2017; Korolev et al. 2017 and references therein). In a multimodel simulation study, Tsushima et al. (2006) showed that the doubling of CO_2 concentrations caused the changes in the distribution of cloud-water in the mixed-phase clouds in a climate simulation to be significant.

PBAPs are solid particles of biological origin and are emitted from the Earth's surface (Després et al. 2012). They are highly active in initiating ice as INPs and include bacteria, fungal spores, pollen, algae, lichens, archaea, viruses, and biological fragments (e.g., leaf litters, insects) and molecules (e.g., proteins, polysaccharides, lipids) (Després et al., 2012; Fröhlich-Nowoisky et al., 2015; Knopf et al., 2011; Szyrmer and Zawadzki, 1997;). Considering the onset temperature of freezing, some ice nucleation active fungi and bacteria (especially *Pseudomonas syringae* with onset freezing temperature around -3^{o}C) are among the most active INPs present in the atmosphere (Després et al. 2012; Hoose and Möhler 2012). The potential impact of PBAP INPs on cloud microphysical characteristics has been recognized for many years; however, this topic remains a subject of debate (DeMott and Prenni 2010; Spracklen and Herald, 2014; Hoose et al. 2010b). Some previous modeling studies have shown that on a global scale PBAPs have only a limited influence on clouds and

precipitation (Hoose et al. 2010; Sesartic et al. 2012, 2013; Spracklen and Heald 2014). On a global scale, the percentage contribution of PBAPs to the immersion freezing (ice nucleation by INP immersed in supercooled water drop) is predicted to be much smaller (0.6%) as compared to dust (87%) and soot (12%) (Hoose et al. 2010).

Many studies have used cloud models to highlight the potential impact of PBAP INPs on cloud microphysics and precipitation (e.g., Levin et al. 1987; Grützun et al. 2008; Phillips et al. 2009). For example, the mesoscale aerosol-cloud model by Phillips et al. (2009) had a 3-D domain of about 100 km in width, and many cloud types were present in the mesoscale convective system that was simulated. Their simulations revealed that the cloud cover, domain radiative fluxes, and surface precipitation rate were significantly altered by boosting organic aerosols representing PBAPs. According to Hummel et al. (2018) in shallow mixed-phase clouds (i.e., altostratus) when the cloud top temperature is below -15^{o}C, PBAPs have the potential to influence the cloud ice phase and produce ice crystals in the absence of other INPs.

The quest for insights into the broader atmospheric role of PBAP INPs for cloud microphysical properties and precipitation is hampered by the limited availability of observations both of their ice nucleation activities for various species and their aerosol distributions in the real atmosphere (Huang et al. 2021). More generally, there is incomplete knowledge about the chemical identity of the key INPs, whether biological or otherwise (Murray et al. 2012). In many global and regional models, the ice nucleation activity of bioaerosols is represented either empirically or theoretically based on laboratory measurements of specific biological species of PBAPs that are assumed as representative candidates (e.g., *Pseudomonas syringae*). This assumption of representativeness introduces uncertainties that would be expected to impact the model results, potentially introducing a

bias into the estimation of the effects of bioaerosols on clouds (e.g. Sahyoun et al., 2016; Hoose et al. 2010b; Spracklen and Herald, 2014, Huang et al. 2021 and references therein).

In addition to primary ice nucleation, ice formation in clouds can occur because of processes generating new particles from pre-existing ice, and these are known as Secondary Ice Production (SIP) mechanisms (Korolev and Leisner, 2020; Korolev et al, 2020). SIP can have a considerable impact on cloud micro- and macro-physical properties such as precipitation rate, glaciation time, cloud lifetime, and cloud electrification by increasing the ice number concentrations by a few orders of magnitude (e.g., Blyth and Latham 1993; Crawford et al., 2012; Lawson et al., 2015; Phillips et al., 2017b, 2018, 2020; Phillips and Patade, 2021; Sotiropoulou et al. 2021a,b). This in turn can influence the global hydrological cycle and climate (Zhao and Liu 2021).

However, in many cloud models, the representations of these SIP mechanisms are uncertain as most of the cloud models include only the Hallet-Mossop (hereafter HM; Hallett and Mossop, 1974) process and neglect other SIP mechanisms (e.g. Fan et 2017; Han et al 2019). A few secondary ice formation processes (e.g., the HM process) have been suggested to be active in the temperature range where active PBAP INPs exhibit strong ice nucleation activity. The INPs of biological origin such as bacteria are highly active in the temperature range of the HM process (-3 to -8^{o}C) as compared with non-biological INPs (Möhler et al. 2008; Patade et al., 2021, henceforth PT21). At temperatures warmer than -15°C, some of the PBAPs generated by biologically active landscapes (e.g. forests, woodlands) can promote ice formation and crystal growth in clouds (Morris et al., 2014).

In the USA, about 18% of the total landmass is used as cropland, farmland, and agricultural activities (Garcia et al. 2012). These are major sources of biological particles in the atmosphere. Biogenic particles released from crops, either pre- and post-harvest, have

previously been shown to serve as INPs (in Colorado and Nebraska, Garcia et al. 2012). Huffman et al. (2013) found that airborne biological particles increase significantly in concentration, by an order of magnitude or more, during rainfall in a forest in the western US and that bioaerosols are well correlated with INPs. Prenni et al. (2013) observed a similar increase in concentrations of ground-level INPs during rain at a forested site in Colorado, which was associated with increased biological particles. Convective clouds can efficiently transport lower tropospheric aerosol particles into the upper troposphere where they can affect the cloud properties (Cui and Carslaw, 2006)

The current study aims to simulate realistic concentrations of multiple groups of PBAP INPs, including bacterial and fungal particles, to investigate their interactions with convective clouds observed during the Midlatitude Continental Convective Clouds Experiment field campaign (MC3E), in the USA (Jensen et al. 2016), in the USA. In view of the literature noted above about the effects of PBAP INPs, there is a need for more detailed analyses of their role in altering cloud microphysical properties and precipitation because the realistic treatment of ice nucleation activity for major PBAP groups was not available, prior to our empirical scheme (PT21). Hitherto, laboratory measurements of isolated biological species (e.g., *Pseudomonas syringae*, *Cladosporium sp*) have been the basis for attempts to simulate biological ice nucleation in clouds, but the representativeness of the choice of such species has been a longstanding issue. For example, Hummel et al (2018) considered three highly ice-nucleation-active PBAP species in their model which may not represent the ice nucleation activity of PBAP in the atmosphere. It is not known which biological species of ice nucleation active (INA) PBAPs contribute the most to biological ice nucleation. Consequently, there is a need for a new approach oriented toward laboratory measurements of biological INPs sampled from the atmosphere, thus optimizing the representativeness of the data for studies of clouds.

In this paper, such an approach is followed to investigate the effect on cloud properties from various major groups of PBAP. We incorporated a recent empirical parameterization for various PBAP groups by PT21 into our 3D aerosol-cloud model (AC). PT21 created an empirical formulation resolving the ice nucleation of each group of PBAPs including 1) fungal spores and their fragments, 2) bacteria and their fragments, 3) pollen and their fragments, 4) detritus of plants, animals, and viruses, and 5) algae. We also examine the relative importance of various secondary ice processes in their role in mediating the PBAP effects on cloud microphysical properties, given the weakness of PBAP effects on cloud microphysical properties.

2. Description of observations

2.1 Selected case of a deep convective system

In the current study, we simulated a squall line that occurred on 20 May 2011 MC3E (Jensen et al. 2016). The MC3E campaign took place from 22 April through to 6 June 2011 and was centered at the Atmospheric Radiation Measurement (ARM) Southern Great Plains (SGP) Central Facility (CF), (36.6◦N, 97.5◦W) in north-central Oklahoma. The surface meteorological analysis on 20 May indicated a southerly flow at the surface, which provided enough moisture from the Gulf of Mexico to trigger convection. Deep convection, organized in the form of a squall line, passed over the measurement site between 1030 and 1100 UTC, resulting in convective precipitation. It was followed by widespread stratiform precipitation that was well observed by both airborne and ground-based measurements. Vertical sounding characteristics of this case are described in Supplement Information (Figure S1) based on the Skew-T plot.

178 *2.2 Aircraft Observations*

179 The *in-situ* cloud microphysical observations used in this study were obtained from a
180 University of North Dakota Citation II aircraft. The aircraft collected observations of cloud
181 microphysical parameters from the cloud base (1.8 km above mean sea level; hereafter MSL)
182 to a maximum altitude of 7.5 kilometres above MSL. The MC3E campaign collected
183 extensive airborne measurements of aerosols and cloud microphysical properties over north-
184 central Oklahoma. A detailed description of the scientific objectives of the MC3E program,
185 including the field experiment strategy, airborne and ground-based instrumentation, is given
186 in the paper by Jensen et al. (2016). A summary of the airborne instrumentation during
187 MC3E is provided in Supplementary Information.

188

189 *2.3 Ground-based measurements*

190 A comprehensive instrumentation suite deployed at the ARM-SGP central facility provided
191 continuous measurements of atmospheric gases, aerosols, clouds, and local meteorological
192 conditions (e.g., wind, temperature, precipitation, and atmospheric profiles). A cloud
193 condensation nuclei (CCN) counter (CCN-100) (DMT) measured the CCN number
194 concentration at seven supersaturation values with a temporal resolution of 1 hour. Surface
195 precipitation was measured with 16 rain gauge pairs placed within a 6-kilometer radius of the
196 SGP CF.

197 During the MC3E campaign, the measurement facility deployed at CF measured the
198 spatial variability of surface fluxes of heat, moisture, and momentum. A radiosonde array of
199 6 sites, covering an area of 300 km × 300 km, was designed to capture the large-scale
200 variability of the atmospheric state. Radiosonde observations (Vaisala RS92-SGP) were
201 conducted with a 6-hour frequency (four times daily) at around 05:30, 11:30, 16:30, and

22:30 UTC, providing vertical profiles of atmospheric state variables (pressure, temperature, humidity, and winds) of the environment surrounding the ARM SGP site. When aircraft operations were planned based on forecasted convective conditions, the sounding frequency was increased to a 3-hour frequency with the starting time at 05:30 UTC.

In addition to airborne observations, the ARM radar network was used to conduct unique radar observations during the MC3E campaign. The information about various radar assets during MC3E is given by Jensen et al. (2016). The surface precipitation used for model validation in this study is a radar-based precipitation estimate as described by Giangrande et al. (2014). Their radar-based rainfall retrievals were in good agreement with observations with an absolute bias of less than 0.5 mm for accumulations less than 20 mm.

The Interagency Monitoring of Protected Visual Environments (IMPROVE) network stations close to the location of airborne observations provided ground-level measurements of various chemical species. These included carbonaceous compounds (black and organic carbon), salt, ammonium sulfate, and dust. The details of the measurement techniques used for mass mixing ratios of these compounds are summarized in Malm et al. (1994). The measurements of these aerosol species from various IMPROVE sites, including Ellis (36.08^{o}N, 99.93^{o}W), Stilwell (35.75^{o}N, 94.66^{o}W), and Wichita Mountains (34.73 ^{o}N, 98.71^{o}W) sites in Oklahoma, were averaged to provide inputs to AC.

Initial mass concentrations for the aerosol species of AC (11 species) including sulfate, sea salt, dust, black carbon, soluble organic, biological and non-biological insoluble organic (five groups of PBAPs) were derived from the Goddard Chemistry Aerosol Radiation and Transport (GOCART) model (Chin et al. 2000). The prescribed mass mixing ratios of aerosol species in A are based on IMPROVE observations and are enlisted in Supplementary Information (Table S2). It should be noted that for the MC3E case considered in this study,

coincident IMPROVE measurements were not available. The mean values of the IMPROVE measurements conducted on May 18 and 21 are used to prescribe the mass of various aerosol species.

3. Methodology

3.1 Model description

The '*aerosol-cloud model*' (AC) used in this study is a cloud-resolving model (CRM) with a hybrid spectral bin/two-moment bulk microphysics, interactive radiation, and semi-prognostic aerosol schemes (Phillips et al. 2017b, 2020). The model predicts the mass and number concentrations for five types of hydrometeors: cloud liquid, cloud ice (or "crystals"), rain, graupel/hail, and snow. The mixing ratios of the total number and mass of all particles in each microphysical species are treated as model prognostic variables. AC treats all known microphysical processes such as droplet nucleation, ice initiation through primary and secondary processes, and growth processes such as deposition/sublimation of ice particles, condensation/evaporation of drops, freezing/melting, as well as coagulation by collisions between various hydrometeor types. Both cloud-base and in-cloud activation of aerosols to form cloud-droplets are treated explicitly, with the predicted in-cloud supersaturation resolved on the model grid being used to activate aerosols aloft. Bin-resolved size distributions of each aerosol species are predicted for the interstitial and immersed components of each aerosol species. Extra prognostic variables track the number of aerosols in each aerosol species that have been lost by INP and CCN activation.

Secondary ice formation is represented by four types of fragmentation:

- breakup in ice–ice collisions (Phillips et al. 2017a, b) (most active between -10 to -20^{o}C);

- Hallett and Mossop (1974), rime splintering (most active between -3 to -8^{o}C);
- fragmentation of freezing rain/drizzle by modes 1 and 2 (Phillips et al. 2018) (most active around -15^{o}C);
- and sublimation breakup (Deshmukh et al. 2021) (most active between -0 to -18^{o}C).

The empirical parameterization (EP) (Phillips et al. 2013) of heterogeneous ice nucleation treats all known modes of ice formation (deposition mode, condensation-/immersion-freezing, inside-out and outside-in contact-freezing) in terms of dependencies on the loading, size, and chemistry of multiple aerosol species. In the previous version of the EP, prior to PT21, there were four species of INP aerosol. One of these was PBAP INPs. However, that version of the EP did not resolve the individual types of PBAP INP, which exhibit a wide range of ice-nucleating abilities. The current version of AC also includes the ice nucleation (IN) activity of dust and black carbon. The ice nucleation parameterization of dust, as well as black carbon, is based on studies by Phillips et al. (2008) and (2013). The activation of dust and black carbon INP starts at temperatures colder than -10 and -15^{o}C.

There are two types of homogeneous freezing represented: that of cloud droplets near -36^{o}C and that of solute aerosols at colder temperatures. Both schemes are described by Phillips et al. (2007, 2009). For cloud droplets, a look-up table from simulations with a spectral bin microphysics parcel model treats the fraction of all supercooled cloud droplets that evaporate without freezing near -36^{o}C, depending on the ascent, initial droplet concentration, and supersaturation. The size dependence of the temperature of homogeneous freezing is represented.

Cloud processes and rainfall formation have been detected using different radar variables, such as specific differential phase K_{DP}. Moisseev et al. (2015), for example, noted an increase in observed K_{DP} because of aggregation. In addition, a few studies have

hypothesized evidence of SIP via K_{DP} (e.g., Sinclair et al. 2016; Kumjian and Lombardo 2017; Carlin et al. 2021). In this study, we attempted to detect secondary ice formation signatures by implementing K_{DP} estimations into AC. Based on Ryzhkov et al. (2011), K_{DP} values were estimated for various hydrometeor types, including cloud drops, raindrops, cloud ice, snow, and graupel (their equations 22, 23, 24, 26, and 29).

3.2 Empirical formulation for PBAP INPs:

In a recent study, PT21 provided an empirical formulation for multiple groups of PBAP INPs based on field observations over the central Amazon. In this study, we modified AC by implementing the recent empirical parameterization of PBAP INPs by PT21. The empirical formulation by PT21 is based on observations of PBAP collected at the Amazon Tall Tower Observatory (ATTO), a research site located in the middle of the Amazon rainforest in northern Brazil. The empirical formulation by PT21 for multiple groups of PBAPs includes: - 1) fungal spores (FNG), 2) bacteria (BCT), 3) pollen (PLN), 4) viral particles, plant/animal detritus (DTS), 5) algae (ALG) and their respective fragments are implemented in AC. This formulation has empirically derived dependencies on the surface area of each group (except algae) and it applies to particles with diameters greater than 0.1 μm. Additional details about the formulation by PT21 are given in Supplementary Information.

3.3 Model setup

AC was driven by initial and evolving boundary data for meteorological conditions. The large-scale advection of humidity and temperature tendencies maintained the convection.

297 Convection was initiated by imposing perturbations onto the initial field of vapour mixing
298 ratio. The large-scale forcing condition used for the simulation was derived using the
299 constrained variational analysis method described in Xie et al (2014). Based on this method,
300 the so-called large-scale forcing including large-scale vertical velocity and advective
301 tendencies of temperature and moisture were derived from the sounding measurements
302 network. During the MC3E campaign, the sounding network consists of five sounding
303 stations centered on a sixth site at the ARM SGP central facility. An area with a diameter of
304 approximately 300 km was covered by this sounding network covers. The supplementary
305 Figure S2 shows the time height evolution of potential temperature and water vapor mixing
306 ratio from large-scale forcing data. It also shows the time variation of CAPE based on
307 observations. The maximum value of CAPE 2400 JKg^{-1} was noticed around 12 UTC on 20^{th}
308 May.

309 The model simulations were carried out for a three-dimension domain of 80 km x 80
310 km with horizontal grid spacings of 2 km. In vertical, the model resolution was 0.5 km, and
311 the model top was located at about 16 km. The lateral boundary conditions are doubly
312 periodic on all sides of the domain. The initial time of the simulations was at 1200 UTC on
313 19 May 2011 and all simulations were performed for 48 hours at a time step of 10 seconds.

314 The GOCART model (Chin et al. 2000) was used to initialize the seven chemical
315 species associated with the EP. The data from the three IMPROVE sites mentioned above
316 (Section 2.3) was used to rescale the mass concentration profiles at all levels so that they
317 match the measurements near the surface. Table S2 in Supplementary Information lists the
318 mass mixing ratios of various aerosol species after the corrections. The corresponding
319 vertical profiles of various aerosol species including sulfate, dust, sea salt, black carbon, and
320 total organic carbon are shown in Supplementary Figure S3 (panel a-e). The corresponding
321 IMPROVE measurements are also shown in the same Figure. There were no direct

measurements of PBAP mass during IMPROVE and therefore it was derived from the measured mass of the total organic carbon (TOC). The relative contribution of insoluble and soluble organic carbon to TOC was assumed to be 20% and 80%, respectively by assuming a water-soluble fraction of 80% for carbonaceous aerosol (Phillips et al. 2017b). AC takes into account the soluble fraction of each type of aerosol. The values of this factor are 0.15 for dust, and 0.8 for carbonaceous species. The value of this fraction for all PBAP groups is 0.1.

There are very few observations available in the literature showing the fraction of PBAP in the insoluble organics or total aerosol particles. For example, observations by Matthias-Maser et al. (2000) found that 25% of the total insoluble particles are biological. PBAPs can contribute a significant fraction to the number concentrations of total aerosol particles (Mattias-Maser et al., 1999). Mattias-Maser and Jaenicke (1995) showed that PBAPs can amount to 20% and 30% of the total aerosol particles. The observation by Jaenicke (2005) in a semi-rural location showed that cellular particles can contribute up to about 50% of total particles. Based on these studies we assumed that 50% of the insoluble organics were biological in origin. The total PBAP loading was prescribed partly based on observations of insoluble organics. The mass fraction of each PBAP group in total PBAP mass is prescribed based on the PT21 observations. The fraction of mass mixing ratio for various PBAP groups is: FNG= 0.39, BCT= 0.13; PLN= 0.31; DTS= 0.17; ALG= 2.5×10^{-4}.

It should be noted that the observations of PBAPs over different geographical locations (including the region where we carried out the simulation) are rare, which prevents us from using the region-specific PBAP observations for the present study. Hence, PT21's default observations were used to calculate the relative contribution of various PBAP groups to insoluble organics. The parameters for the shape of PSD of each PBAP group (modal mean

346 diameters, standard deviation ratios, and relative numbers in various modes) are prescribed
347 based on observations from Amazon (PT21). Supplementary Figure S4 depicts the
348 corresponding size distribution of various PBAP groups in AC. To check the validity of the
349 observation from PT21 over the region considered in the current study, the model estimated
350 values of one of the major PBAP bacteria are compared with the observations as shown in
351 Supplementary Figure S5. It shows that the estimated values of bacterial number
352 concentration are overall in fair agreement with previous observations (e.g. Bowers et al
353 2009; Bauer et al. 2002; Burrows et al. 2009). The simulated bacterial (~ 10^4 m^{-3}) and fungal
354 (~ 10^3 m^{-3}) number concentration by AC is in good agreement with their typical
355 concentration in the atmosphere (Després et al. 2012). The resulted vertical profiles of mass
356 of the various PBAP groups are shown in Figure S3 (panel f).

357 From these prescribed loadings of aerosol species, AC predicts their size distribution
358 and hence the CCN activity spectrum. Using the initial sounding and aerosol profile, AC can
359 predict the in-cloud size distribution of aerosols in each species as well as in-cloud
360 supersaturation. Figure S6 in Supplementary Information shows the predicted CCN spectrum
361 comparison with observations from the CCN counter at the surface at the SGP site. It should
362 be noted that the aerosol mass loading from IMPROVE observations showed variations of
363 20-30% for the simulated case. The uncertainties in the input aerosol mass loading can result
364 in simulated CCN concentration and are shown by the errors in the CCN concentration
365 predicted by the AC. During 19-20 May, the measured number concentration of active CCN
366 at the SGP CF ranged from 400 to 3000 cm^{-3} at 1% supersaturation (Fridlind et al. 2017). The
367 measurements were made on 20 May before the start of the rain in clear air. The normalized
368 CCN number concentrations at 1% supersaturation from observations and AC are ~ 1000 cm^{-3}
369 and ~ 940 cm^{-3}, respectively. Given the wide range of observed CCN concentrations at each

supersaturation as well as the uncertainties in the model predicted CCN concentration, the predicted and observed CCN activity spectra are in acceptable agreement.

4. Results from control simulation and model validation

4.1 Overview of the control simulation

An intense north-to-south oriented squall line moved over the ARM SGP CF on May 20, 2011, from 1100 to 1400 UTC (Sec. 2.1). The new version of AC simulated this case, after implementing the empirical formulation by PT21 for multiple groups of PBAP INPs ('control' simulation) (Sec. 3). It should be noted that five ensemble runs were carried out for control simulation (See Table S3 in Supplement Information) varying the perturbing in the initial water vapor mixing ratio.

Figure 1 shows the time-height evolution of various liquid and ice cloud microphysical parameters derived from the control simulation conditionally averaged over cloudy regions. The maximum average cloud droplet number concentration was around 250 cm^{-3}. The LWC was typically less than 0.5 g m^{-3}. The freezing level (0^oC) was around 4.1 km above MSL. The deep convection began around 10 UTC, followed by intense precipitation around 11 UTC, and reached its peak around 12 UTC. The time-height evolution of cloud ice, snow, and graupel number concentrations shows maxima shortly before 12 UTC, which coincides with the time of peak precipitation. This suggests that the ice phase was important in precipitation formation.

The time-height map of simulated radar reflectivity during 20 May, unconditionally averaged over the whole domain is shown in Figure 1g. It shows the well-defined squall line passing over the domain from 1100 to 1500 UTC. The maximum of this domain-wide

simulated reflectivity is around 40 dBZ when deep convection was happening. The instantaneous maximum of reflectivity at any grid-point (not shown here) was about 50 dBZ. At other times, the average reflectivity was typical of the stratiform cloud of about 15 dBZ. The cloud top height of the squall line decreases after 1400 UTC.

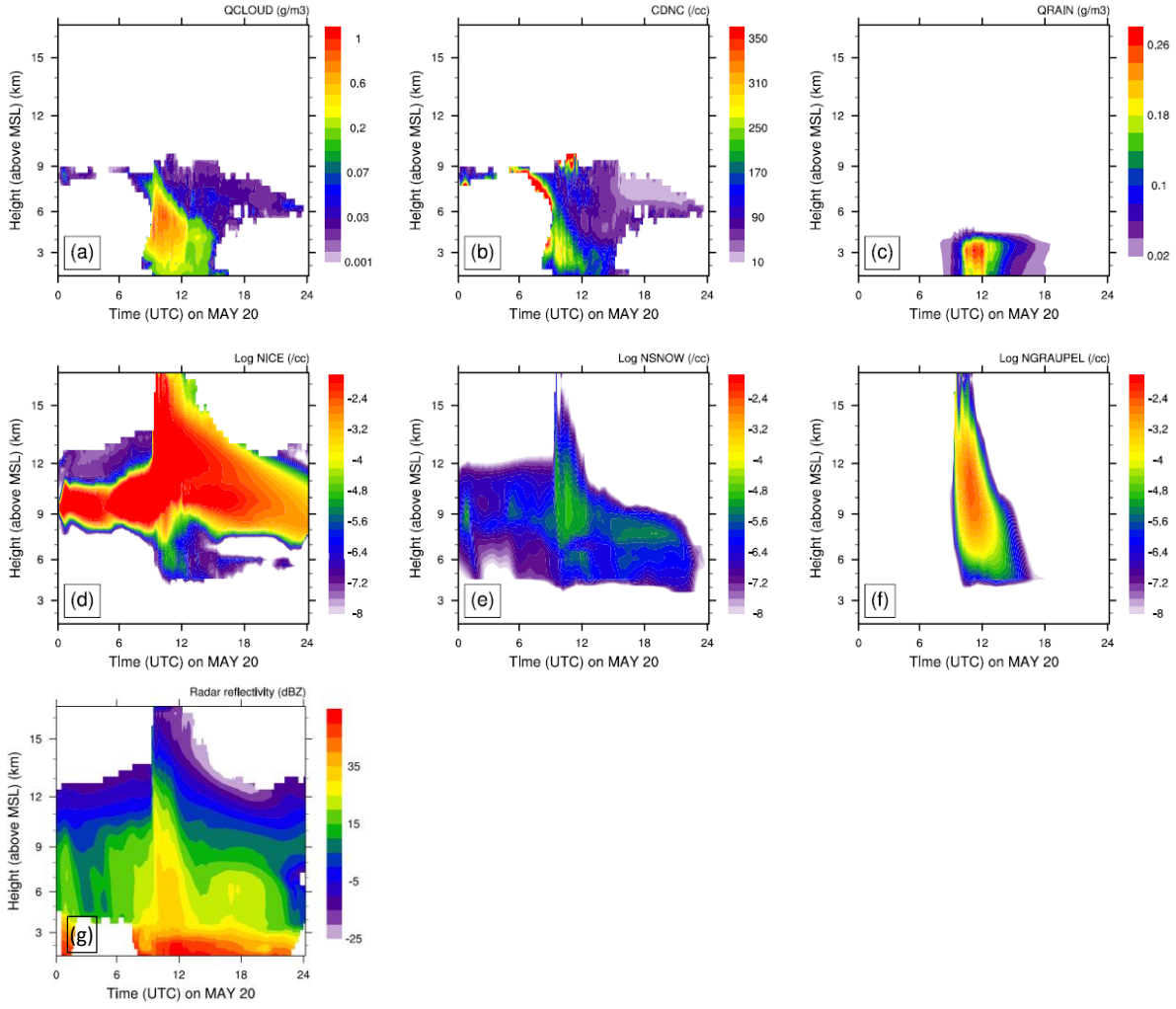

Figure 1: Time-height contours of domain averaged a) cloud water mixing ratio (QCLOUD); b) cloud droplet number concentration (CDNC); c) rainwater mixing ratio (QRAIN); d) number concentration of cloud ice (NICE); e) number concentration of snow (NSNOW); f) number concentration of graupel (NGRAUPEL). Due to a wide range of values, the log values number concentrations are plotted. The surface height is ~ 500 m. The averaging was done for cloud points with LWC > 0.001gm^{-3} or total water content (TWC)> 10^{-6} gm^{-3}. Also shown is the time-height evolution of domain averaged (g) radar reflectivity.

4.2. Model validation against coincident observations of the storm

The extended stratiform region of the squall line while in the vicinity of the SGP CF was sampled by the Citation aircraft equipped with a full suite of cloud microphysical instrumentation. The aircraft started sampling the stratiform precipitation region at around 1300 UTC and continued the observations at sub-freezing temperatures from 1335 to 1515 UTC. Occasionally, the aircraft encountered weak convective updrafts (< 6 m/s). The aircraft actively avoided convection that was more vigorous than that. In this section, we validate various microphysical and dynamical quantities from the control simulation against aircraft and ground measurements. The control run includes all primary and SIP processes of ice initiation. The vertical profiles shown here are an average of five ensemble runs.

Figure 2 compares the aircraft observations against predicted microphysical quantities, with both the predictions and observations identically averaged, conditionally over convective ($6 > |w| > 1$ m/s) and stratiform regions ($|w| < 1$ m/s). The simulated LWC decreases exponentially with height above the cloud base. There is considerable scatter in observed LWC at each level. The various degrees of dilution of sampled parts of the cloud can cause these variations in LWC at a given altitude. The maximum simulated LWC of 0.5 gm^{-3} was observed in the convective region at temperatures warmer than -5^{o}C. In the convective region around -5^{o}C, the measured LWC is lower than the simulated LWC by a factor of 3. For the stratiform region, simulated values of LWC are in adequate agreement with observations. Overall, the means of observed LWC are in acceptable agreement with the model results for convective as well as stratiform regions.

The vertical profiles of simulated and observed Cloud Drop Number Concentration (CDNC) (Fig. 2c and 2d) showed that CDNC was lower than 300 cm^{-3}. In the convective region, the measured CDNC is 40% lower than the simulated CDNC at 15^{o}C. However, an

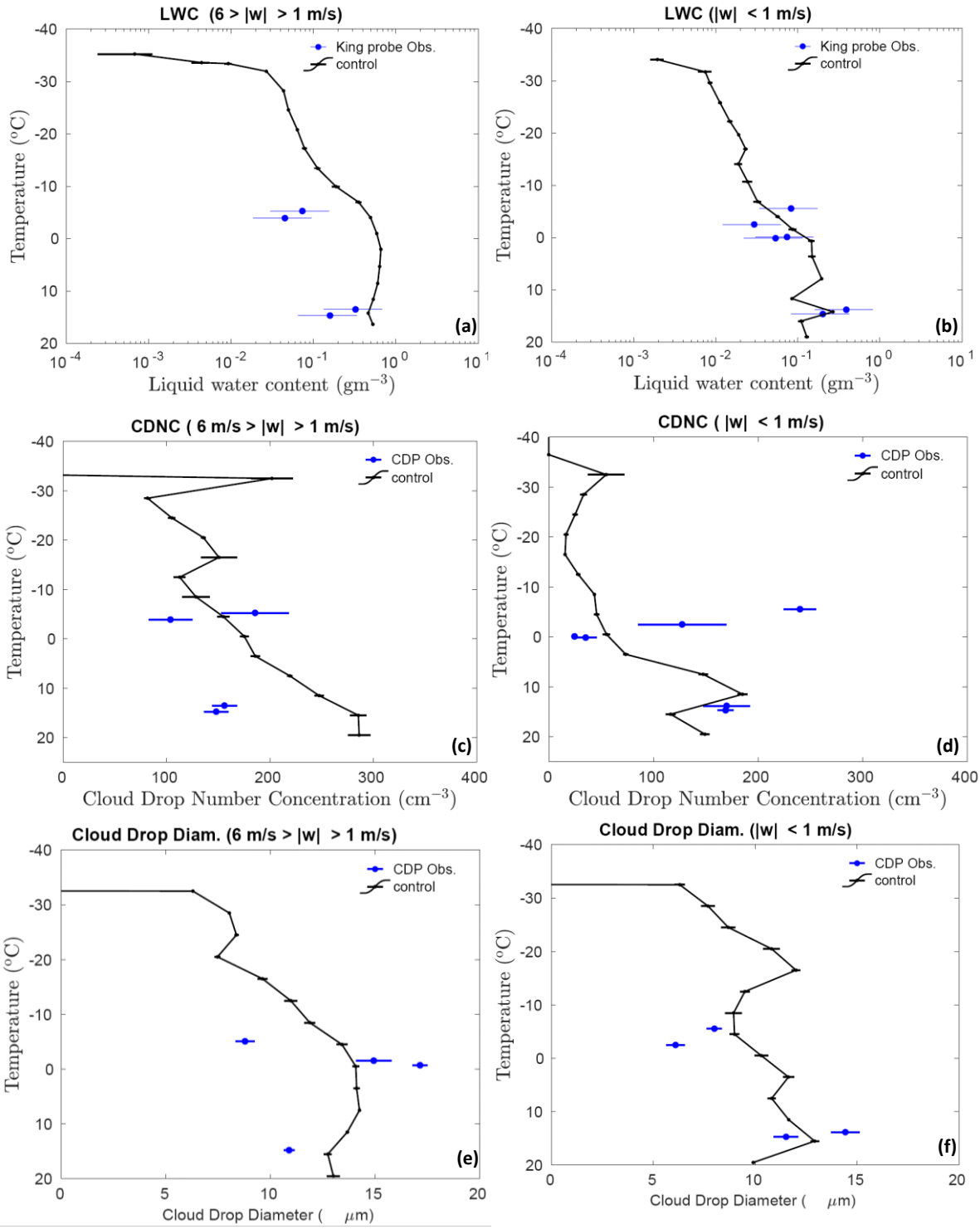

Figure 2: Comparison of the control simulations by AC with aircraft observations, for liquid water content conditionally averaged over (a) convective (6 m/s > $|w|$ > 1 m/s) and (b) stratiform ($|w|$ < 1 m/s) regions; cloud drop number concentration over (c) convective and (d) stratiform regions; average size of cloud droplets (< 20 μm) conditionally averaged over (e) convective and (f) stratiform regions. All the vertical profiles shown here are averaged for the whole domain. The error bars were estimated based on five ensemble runs.

adequate agreement between them is found around -5^{o}C. For the stratiform region, simulated CDNC is much higher in the mixed-phase region. However, at a temperature warmer than 0^{o}C the values of observed CDNC are in acceptable agreement with observations. The observed and simulated mean diameter of cloud droplets varied between 6 to 16 μm (Figures 2e and 2f). There are few points in the convective region e.g., around -5^{o}C, where the observed cloud drop diameter is 50% lower than the simulated value. An adequate agreement between simulated and observed cloud drop diameter was found for the stratiform region. Overall, the predictions of average CDNC and cloud droplet diameter, in both convective and stratiform regions, show a fair agreement with observations.

The ice particle number concentration from observations and the control simulation is also compared as shown in Figures 3a and 3b for convective and stratiform regions, respectively. It should be noted that the observed number concentration of ice particle particles smaller than 200 μm is prone to shattering, even with the use of the shattering correction algorithm. This can introduce a significant bias in the observed ice number concentration (Korolev et al., 1991). To avoid these biases, we have compared the number concentration of ice particles with a diameter greater than 200 μm from both observation and model (denoted by 'NT200'). However, in the rest of the manuscript (in sensitivity studies), the number concentration from the model included ice particles of all size ranges.

Observations show that the concentration of ice particles gradually increases as the temperature decreases, as expected. The maximum ice number concentration from the aircraft observations (with D > 200 μm) is ~ 0.06 cm^{-3} around -15 ^{o}C. Good agreement to within 50% at most levels, was found between the model simulated NT200 and that observed for the convective region.

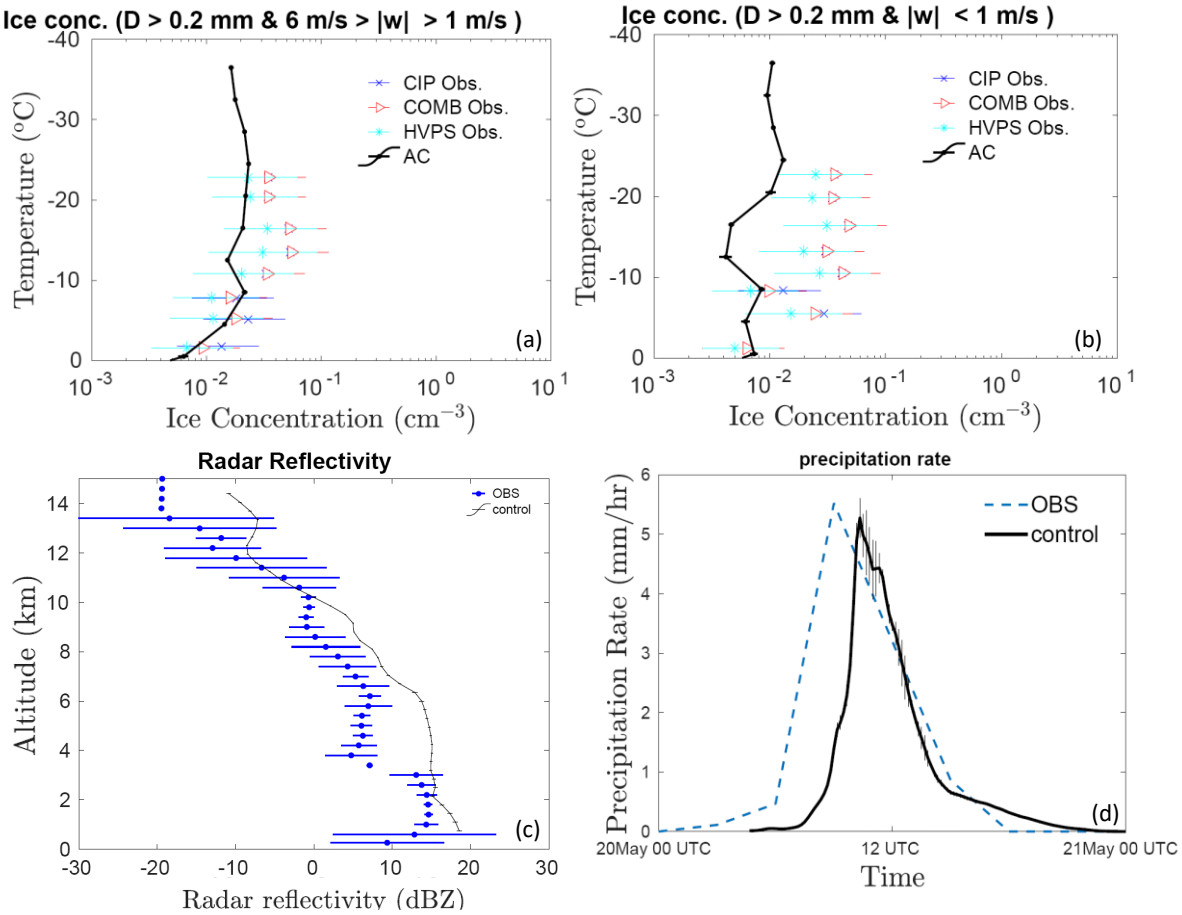

Figure 3: Comparison of the control simulations by AC with aircraft observations, for ice number concentration of all particles > 0.2 (NT200) mm in the maximum dimension of all microphysical species (cloud ice, graupel/hail, snow), averaged over (a) convective (6 m/s > $|w|$ > 1 m/s) and (b) stratiform ($|w|$ < 1 m/s) regions. (c) The vertical profile of simulated radar reflectivity conditionally averaged over all regions of significant reflectivity (> -20 dBZ) at each level is compared with observations from ground-based radars. The temperature corresponding to each altitude is mentioned on the right axes; (d) predicted precipitation rate (mm/hr) compared with ground observations at the SGP CF. All the vertical profiles shown here are averaged for the whole domain. The error bars were estimated based on five ensemble runs.

In the stratiform region, at most levels, model values of NT200 have the same order of magnitude as observations. However, between about the -10 and -16°C levels, the stratiform NT200 values are about half an order of magnitude lower than the observations. In similar simulations of the 20 May case, Fan et al. (2015) and Fridlind et al. (2017) also showed underestimation of simulated ice number concentrations. Compared to observations,

their simulations showed half an order of magnitude bias in ice crystal number concentration. Comparatively, for the convective region, our model predicted ice number concentrations were in better agreement with observations. As mentioned in section 2.2, imaging probe data is prone to shattering, and various corrections were used to rectify it. However, there are currently no ways to determine how many undetected artifacts remain after shattering corrections have been applied (Baumgardner et al. 2022). Such uncertainties in measured ice number concentration could result in such bias in observed and simulated ice number concentrations. In summary, though the AC model is not totally perfect, it did a fair job in simulating observed ice number concentrations.

In Figure 3c, the radar reflectivity from vertically pointing Ka-band ARM zenith radar is compared with the mean profile from model simulations. This figure illustrates that simulated reflectivity profiles below roughly 3 km and above 8 km MSL altitudes are in good agreement with observations. Between 3 and 8 km MSL (temperatures of 2 and -30^{o}C), the bias in reflectivity from model simulations and observations is about 10 dBZ. Thus, the simulated reflectivity is substantially higher than observed, particularly at levels where the aircraft sampled the clouds. Fridlind et al. (2017), as well as Fan et al. (2015), noticed similar overestimations of reflectivity within stratiform outflow of the squall line case on 20 May. They attributed the reflectivity biases to significantly larger ice particles in the simulations than observed.

Figure 3d compares the time series of precipitation rate from the control simulation with the radar-based precipitation estimates. In both, control simulation and observations, a maximum precipitation rate of about 5 mm/hr was noticed, with an error in the prediction of less than 5%. In comparison to observations, the simulated squall line arrives 1-2 hours later. The lack of resolution of the 3D turbulence in the planetary Boundary Layer and uncertainties

503 associated with the 3D structure of initial and boundary conditions can all have an
504 independent impact on the simulated rainfall structure, resulting in a delayed peak.
505 Nonetheless, AC has done a fair job in simulating the peak in the predicted precipitation rate.

506

507 *4.3 Analysis of simulation with ice particle budgets and tagging tracers*

508 The activated PBAP INPs from the control run are shown in Figure 4 for the convective and
509 stratiform regions. In addition to the PBAP INPs, Figure 4 also shows the activated INPs
510 from dust and black carbon. It should be noted that these concentrations shown here are based
511 on advective tagging tracers that follow the diffusion, ascent, and descent inside cloud
512 motions. Overall, bacterial, and fungal particles dominate the biological INP concentration in
513 the simulated cloud. For example, at -20^{o}C the activated INPs from bacteria and fungi are
514 higher than the other three groups of PBAP INPs (detritus, pollen, algal) by two orders of
515 magnitude in both convective as well as stratiform regions. At that level in convective
516 regions, the average concentration of simulated active PBAP INPs is about 3×10^{-6} cm^{-3},
517 which is two orders of magnitude less than the maximum total for all active INPs (about
518 3×10^{-4} cm^{-3}) in the whole simulation. Overall, the predicted total INP concentration is
519 dominated by black carbon and dust. At -10^{o}C, the Activated INPs from dust and black
520 carbon differ by an order of magnitude from the total PBAP INPs in convection.

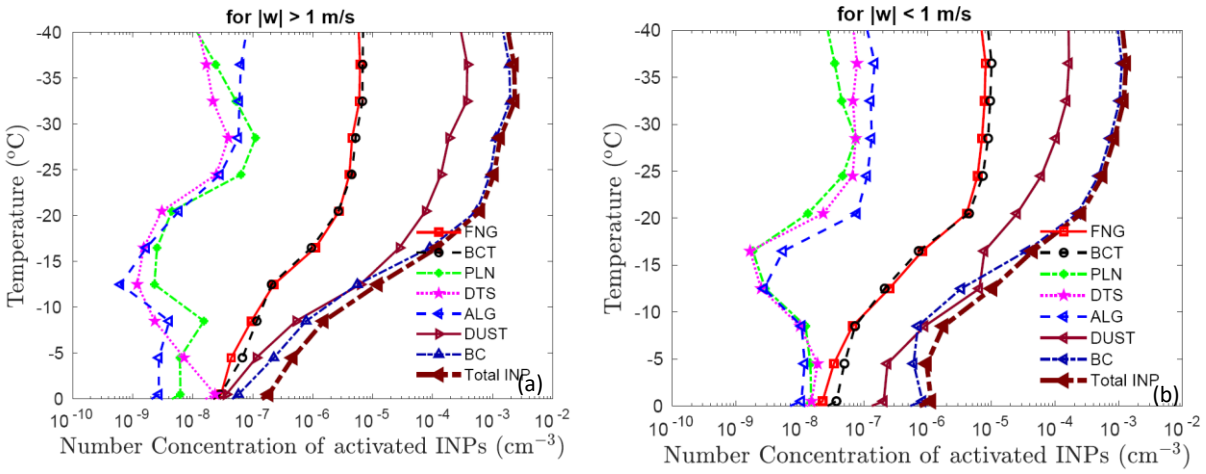

Figure 4: The activated number concentration INPs from various PBAP groups along with dust (DUST) and black carbon (BC) and total INPs at various temperatures for (a) convective and (b) stratiform regions. All the vertical profiles shown here are averaged for the whole domain.

The formation of ice in a cloud is a result of several primary and secondary processes. It is important to understand the relative importance of these processes in precipitation formation. To that end, Figure 5a shows the ice particles initiated from various sources throughout the 3D domain of the entire simulation. The primary homogeneous (PRIM_HOM) dominates the total ice budget. Among all SIP mechanisms, breakup caused by collisions between various ice particles is the most important in determining total ice number concentration. The ice production by sublimation breakup of graupel is slightly lower than PRIM_HOM. However, the contribution of ice production via sublimation breakup of dendritic ice crystals is negligible.

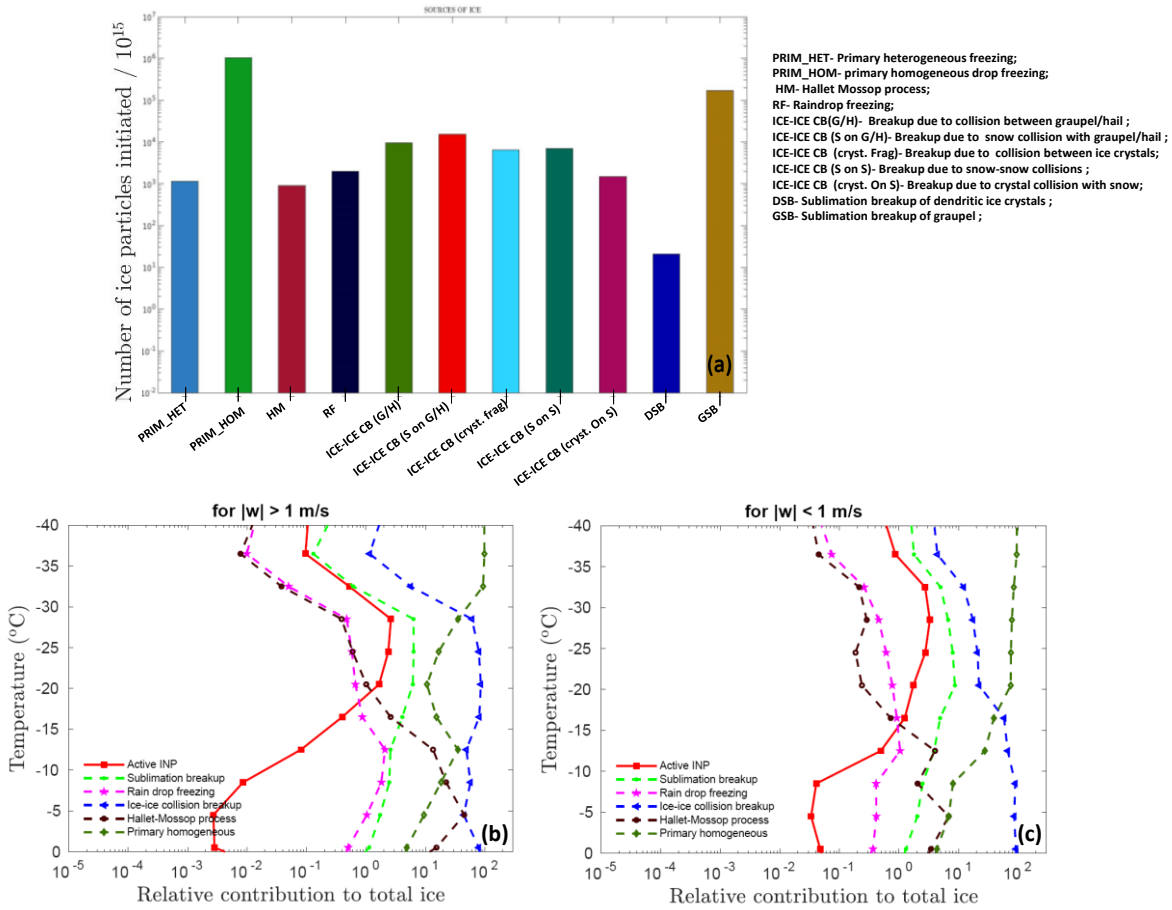

Figure 5: (a) Ice crystal budget for simulated MC3E case. The number of ice crystals produced by various mechanisms (as shown in the legend box) per 10^{15} particles is shown. Also shown is the relative contribution of various SIP mechanisms such as sublimation breakup, raindrop freezing, ice-ice collision breakup, and the Hallett-Mossop process to the total ice number concentration as a function of temperature, averaged conditionally over only (b) convective and (c) stratiform regions. The relative contribution was calculated based on advective tagging tracers for the given process. The convective and stratiform regions were identified based on criteria $|w| > 1$ and $|w| < 1$, respectively.

Figure 5b and 5c depict the relative importance of ice concentration from various SIP mechanisms, as well as active INPs in determining total ice number as a function of temperature for convective and stratiform regions. Each source of ice displayed is tracked with advective "tagging tracers" throughout the simulation. Overall, at temperatures warmer than -15°C, the contribution to the total ice number concentration from various SIP is 2-3

555 orders of magnitude higher than the concentration of active INPs, highlighting the importance
556 of SIP mechanisms in ice formation. At -25^{o}C, breakup in ice-ice collisions contributes
557 around 75% and 20% of the total ice concentration in the convective and stratiform regions,
558 respectively. At the same temperature, in both convective and stratiform regions, sublimation
559 breakup and raindrop freezing contribute about 8% and 0.8 %, respectively. It can be
560 observed that in the convective regions at temperatures warmer than -30^{o}C, SIP mechanisms
561 are important in determining the total ice concentrations, whereas at colder temperatures
562 homogeneous nucleation is dominant. In the stratiform region, this crossover occurs at a
563 much warmer temperature around -18^{o}C. At temperatures colder than this homogeneous
564 nucleation is a major contributor to the total ice whereas at warmer temperatures SIP
565 mechanisms prevail. Overall, the contribution of active INP to the total ice is lower than 3%.

566 Secondary ice formation via the HM process of rime-splintering contributes
567 significantly to ice production at temperatures warmer than about -15 ^{o}C (Fig. 5b and 5c),
568 enhancing the ice concentration beyond the primary ice. In the convective region, the
569 contribution of the HM process in total ice can reach as high as 40% around -5^{o}C. The
570 simulated cloud droplet diameter is mostly smaller than 15 μm. It is smaller than the cloud
571 droplet size required for the HM process to occur. In AC, the rate of the rime-splintering
572 mechanism depends on the concentration of droplets > 24 μm. It should be noted that in the
573 AC model HM process is treated with a factor multiplying the fragment emission which
574 depends on the cloud droplet size. This factor is zero for cloud diameter below 16 μm and
575 unity above 24 μm with linearly interpolated in between.

576

577 **5. Results from sensitivity tests about the influence of PBAP**

578 To quantify the effect of multiple types of PBAPs on cloud properties, sensitivity tests were
579 performed by modifying the control simulation and comparing the perturbed simulations with
580 it. Description of various sensitivity tests carried out in the current study are enlisted in
581 Supplementary Information (Table S3). The corresponding figures for each simulation are
582 also mentioned.

583 Simulations were performed by eliminating all PBAPs from the control (‘*no-PBAP’*
584 case) and by multiplying their initial loadings at all levels by factors of 10 and 100 (‘*high-*
585 *PBAP’* and ‘*very high-PBAP’* cases) respectively. Comparison with the control simulation
586 reveals the overall effect from both the CCN and IN activities of all bioaerosols combined.
587 These factors are justified by considering the variations in PBAP concentrations in the range
588 of about 0.1 to 30 L^{-1} over North American forests (Huffman et al. 2013). An additional
589 simulation was conducted with a 1000-fold increase in initial PBAP loading (‘*ultra high-*
590 *PBAP*’) to investigate if these unrealistically high concentrations of PBAPs could affect the
591 ice phase in a purely hypothetical scenario. Five ensemble runs were carried out for all major
592 simulations involving perturbations in PBAP loading. The ensemble runs were carried out by
593 varying the perturbation in initial conditions (water vapor mixing ratio).

594 Additional simulations were performed by removing treatment of biological IN
595 activity in the EP (‘*no-PBAP INP*’ case) relative to the control run. A comparison of both
596 additional simulations against the corresponding simulations with the full change in the
597 PBAP loadings (no-PBAP and high-PBAP cases) reveals the separate roles of the INP and
598 CCN activities for the changes in biological material. Apart from these changes in PBAPs,
599 the perturbed simulations are identical to the control run.

600 Figure 6 reveals the effects of all bioaerosols on cloud properties in the convective
601 region ($|w| > 1$ m/s). Overall, changes in cloud microphysical properties including liquid
602 water content, cloud droplet size, cloud drop number concentration, ice number concentration

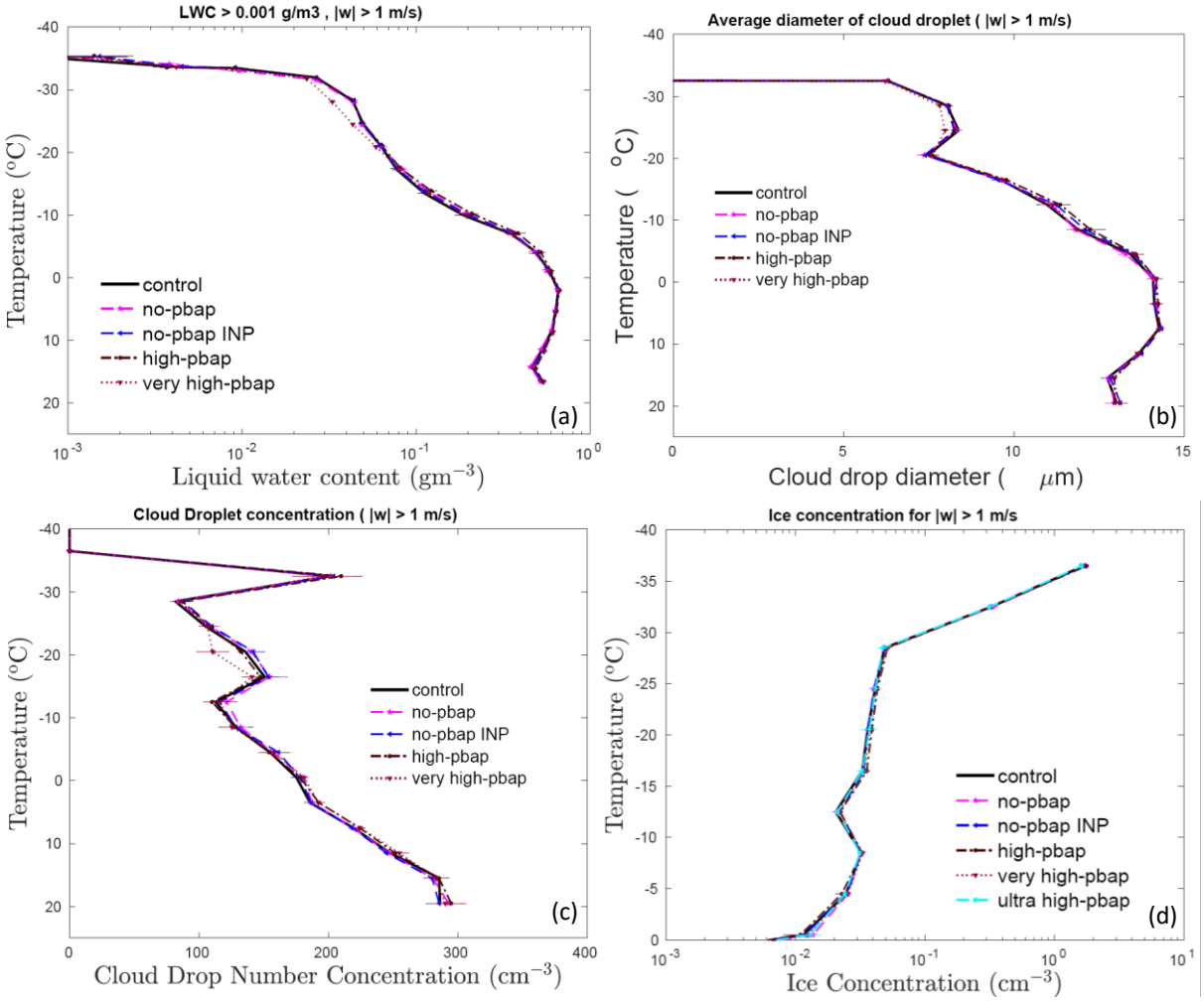

Figure 6: The temperature dependence of the (a) liquid water content, the (b) cloud droplet number, (c) the cloud droplet diameter, and the (d) total ice number concentration for 'control' simulation and various sensitivity runs involving a change in total PBAP number concentrations for in the convective region. The averaging conditions are mentioned at the top of each figure. The ice number concentration from the ultra high-PBAP is also shown in panel d. All the vertical profiles shown here are averaged for the whole domain.

are less sensitive to the changes in PBAPs for the convective part of the simulated clouds and are not statistically significant. The LWC, cloud droplet number, and cloud drop diameter in the perturbed simulations do not differ much (< 3%) from the control run. For the whole storm, considerable changes in the spatial distribution of total ice number concentration are observed due to changes in PBAPs (see Supplementary Figure S7). However, vertical profiles showed very small changes in the ice number concentrations. In the convective region,

changes in ice crystal number concentration due to changes in PBAPs are negligible (< 6%). This includes the extreme changes in bioaerosol loading (ultra high-PBAP case).

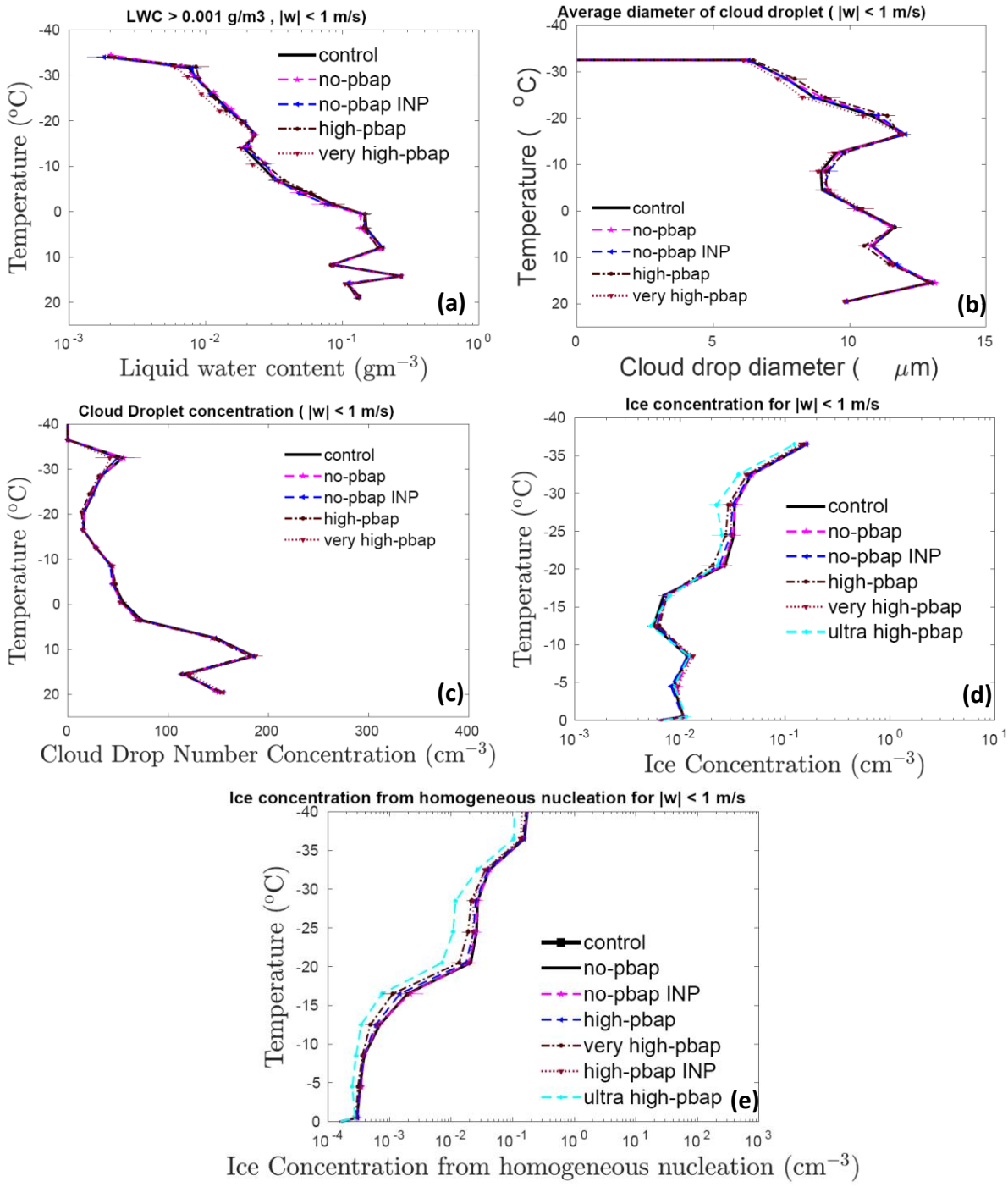

Figure 7: The temperature dependence of (a) the liquid water content, (b) the cloud droplet number, (c) the cloud droplet diameter, and the (d) total ice number concentration for 'control' simulation and various sensitivity runs involving a change in total PBAP number concentrations for in the stratiform region. Also shown is the temperature dependence of (e) ice concentration from homogeneous freezing. The averaging conditions are mentioned at the top of each figure. The total ice number concentration and ice number from homogeneous

freezing from ultra high-PBAP are also shown in panels d and e. All the vertical profiles shown here are averaged for the whole domain. The error bars are based on ensemble runs.

Figure 7 shows the corresponding effects in the stratiform region ($|w| < 1$ m/s) from all bioaerosols. The changes in warm microphysical properties because of changes in PBAP loadings are smaller than 10%. In this part of the cloud, the ice-microphysical parameters are comparatively more sensitive to the changes in PBAP than in the convective region. The ultra high-pbap case predicted ~40% lower ice number concentration than the control run. However, these changes in ice number concentration are not significant as the error bars associated with ensemble members overlap. For the stratiform region, all other simulations considered here showed < 10% change in ice number concentrations compared to the control run. These changes in ice number concentration due to PBAPs are mostly controlled through their effect on homogeneous freezing above the -36^{o}C level as shown in Figure 7e by tagging tracer for homogeneous nucleation. These ice particles can then advect to lower levels affecting ice number concentrations in the mixed-phase region.

Figure 8 shows the number of ice particles generated by homogeneous nucleation, various mechanisms of primary nucleation (8a), and secondary ice production (8b) per 10^{15} ice particles for the entire storm. Homogeneous freezing dominates the ice production among the three broad types of ice formation mechanisms (heterogeneous and homogeneous ice nucleation, SIP). The maximum changes in ice nucleated through the primary ice mechanism are noticed for the very high-PBAP case and can be attributed to the 100-fold increase in all PBAP loading. The very high-PBAP simulation predicted a 15% lower number of homogeneously nucleated ice than the control run. The very high-PBAP cases predicted about 80% more primary ice crystals formed at temperatures warmer than -30^{o}C. At temperatures colder than -30^{o}C, this case predicted 20% more primary ice crystals than the control run. The very high pbap case showed an increase in primary heterogeneous ice and a

decrease in primary homogenous ice. Since the contribution of primary homogenous ice nucleation is much higher in determining the total ice number concentration when compared with primary homogeneous nucleation, the overall effect of the very high pbap case is a decrease in total ice number concentration as shown in Figure 7 and Table S4 in the Supplementary Information. However, at temperatures warmer than -35°C, ice number concetration in the very high pbap case was comparable with the control run (Table S5).

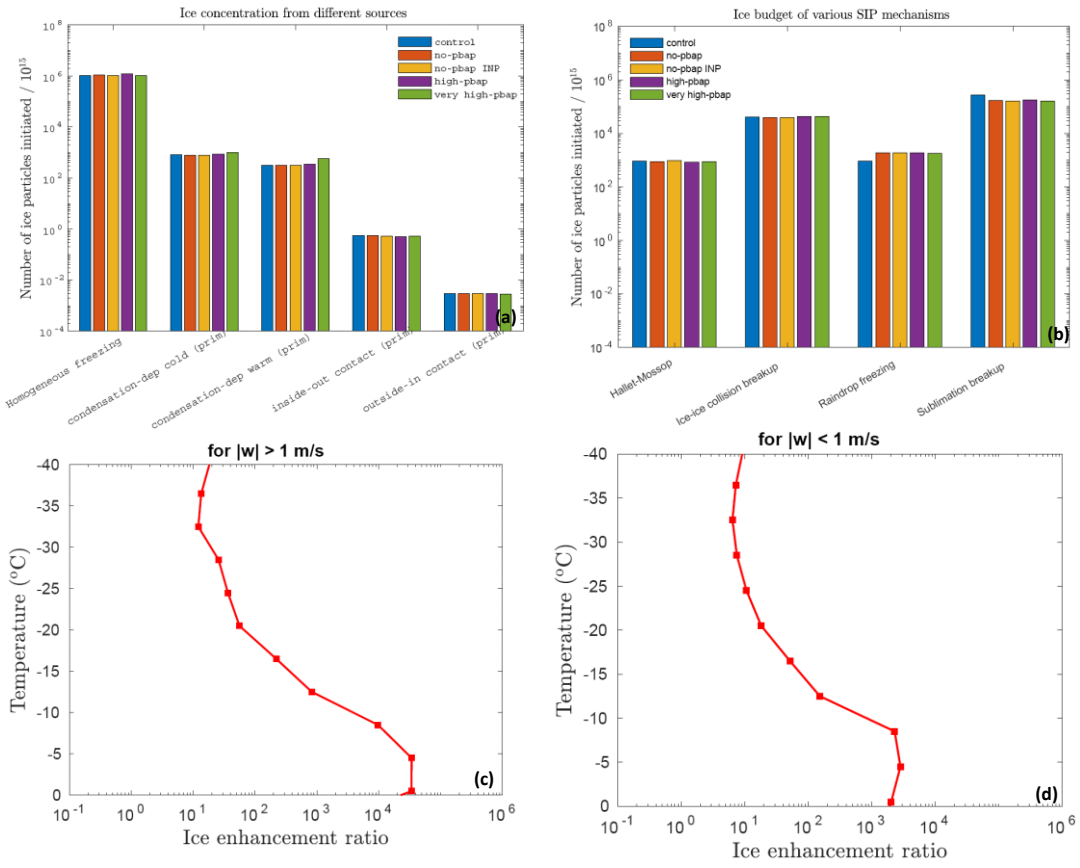

Figure 8: The number of ice crystals produced during the whole storm by (a) primary ice nucleation mechanisms and homogeneous freezing as well as (b) various SIP mechanisms (as shown in the legend box) per 10^{15} particles is shown for various sensitivity runs. The ice enhancement ratio for the convective and stratiform regions is shown in 8c and 8d.

667 Figure 8b shows that among SIP mechanisms, the contributions of ice-ice collision
668 breakup and sublimation breakup are higher by an order of magnitude than the HM process
669 and raindrop fragmentation. However, the budget analysis (not shown in the plot) showed
670 that about 75% of the fragments associated with sublimation breakup are prone to
671 evaporation, making ice-ice collision breakup a major SIP mechanism. The estimated ice
672 enhancement ratio, which is a ratio between the number concentrations of total ice (excluding
673 homogeneous nucleation) and primary ice, is shown in Figures 8c and 8d for convective and
674 stratiform regions respectively. Overall, the ice enhancement ratio varied between 10 to 10^4
675 which indicates the importance of SIP mechanisms. The budget analysis shows that overall,
676 the perturbations in bioaerosols resulted in very small changes (with maximum change <
677 40%) in ice generated by SIP mechanisms.
678 The role of PBAPs in altering radar reflectivity and surface precipitation was limited
679 and described briefly in Supplementary material (Figure S8). The overall effect of PBAPs on
680 accumulated surface precipitation was minimal (< 4%) (Figure S8 and Table S4). In addition,
681 the changes in PBAPs do not show a significant impact on shortwave and longwave radiation
682 fluxes as well cloud fractions as discussed in the Supplementary information (Figure S9).
683

684 **6. Results from sensitivity tests about secondary ice production**

685 Various sensitivity experiments were conducted to evaluate the role of SIP mechanisms in
686 determining micro- and macrophysical parameters of the clouds (See Table S3). SIP through
687 sublimation breakup and breakup in ice-ice collisions were switched off in the 'no-
688 sublimation breakup' and 'no-collisional ice-ice breakup' simulations, respectively. In the ‘no-
689 secondary' case, no SIP mechanisms were active.

690 The results from these sensitivity experiments are shown in Figure 9 for the
691 convective as well as the stratiform region of the simulated cloud. Overall, in the convective
692 region, the no-secondary and no-collisional ice-ice breakup cases predicted 5 and 12% higher
693 LWC respectively, than the control run (See Table S4 in Supplementary Information). In the
694 stratiform region, these cases predicted ~25% higher LWC than the control run. Lower ice
695 number concentrations due to the absence of SIP mechanisms may reduce the rate of
696 conversion of liquid to ice via mixed-phase processes, resulting in a higher LWC.

697 In the convective part, the absence of any SIP increased ice number concentration by
698 half an order of magnitude at temperatures warmer than -25^{o}C. Comparing the no-SIP and
699 control cases, the effect of the inclusion of SIP mechanisms is to increase the average ice
700 concentration by up to half an order of magnitude at temperatures warmer than -15^{o}C in the
701 stratiform region. For the stratiform region, at temperatures colder than this, the absence of
702 SIP mechanisms resulted in higher ice number concentrations by a similar magnitude. These
703 changes at the colder levels are associated with homogeneous droplet freezing. The changes
704 in ice number concentration in the no-collisional ice-ice breakup case are comparable with
705 the no-secondary case. Compared to break up in ice-ice collisions, sublimation breakup has a
706 lower impact (< 40%) on the total ice number concentration in both convective and stratiform
707 regions.

708 The changes in simulated radar reflectivity, total specific differential phase, and
709 surface precipitation rate with SIP mechanisms are shown in Figures 9e, 9f, and 9g,
710 respectively for the whole storm. Overall, the simulated radar reflectivity was 1 dBZ lower in
711 the no-SIP and no-collisional ice-ice breakup case than in the control run and can be
712 attributed to the overall increase in ice number concentration in the control run.

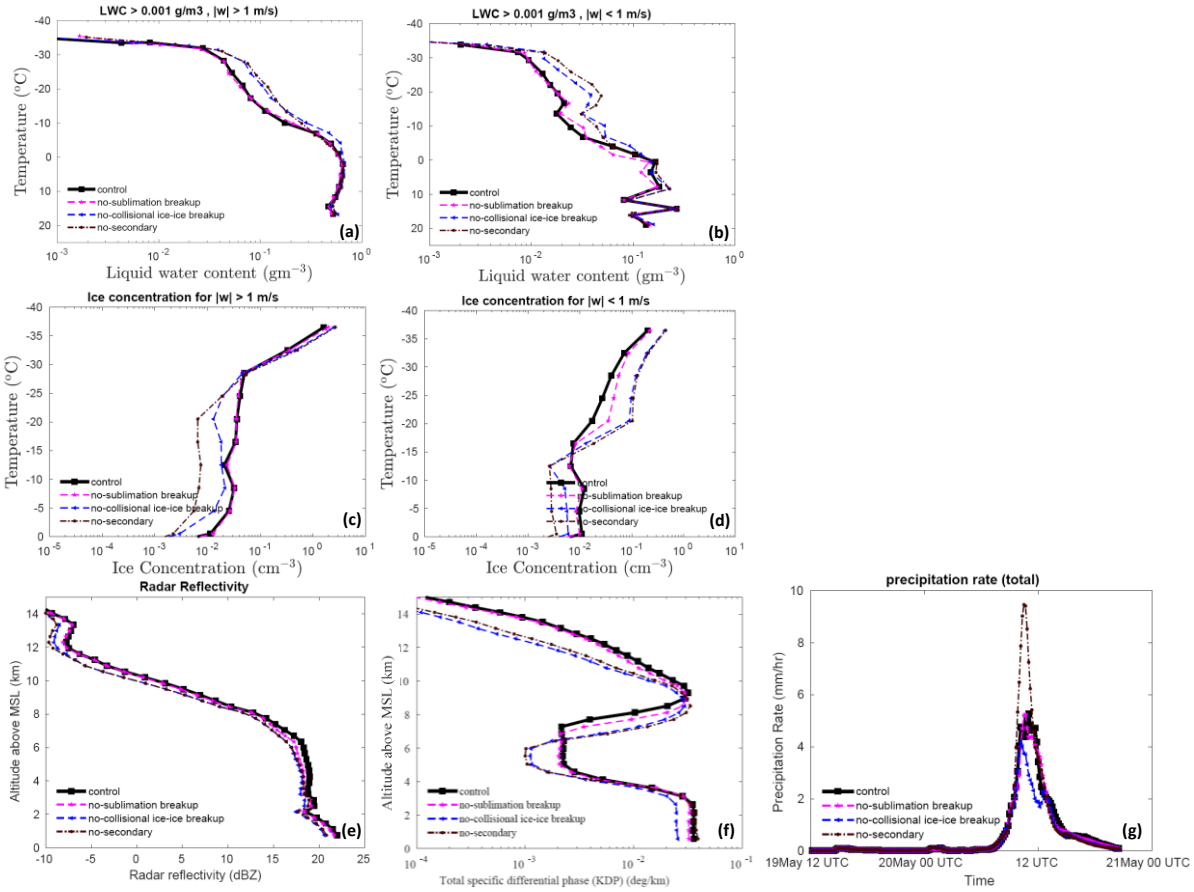

Figure 9: Temperature dependence of the liquid water content in (a) the convective and (b) the stratiform region for 'control' simulation and various sensitivity runs involving SIPs. The ice number concentration is also shown for the (c) convective and (d) stratiform regions. The averaging conditions are mentioned at the top of each figure. The vertical profiles of (e) radar reflectivity, and (f) total specific differential phase are also shown for the same simulations. (g) The temporal evolution of the total surface precipitation rate averaged over the domain is also shown. All the vertical profiles shown here are averaged for the whole domain.

The no-sublimation case predicted slightly higher reflectivity than the control run. The absence of all SIPs resulted in about a 100% decrease in the K_{DP} at a temperature colder than -40^{o}C. Between -10^{o}C to -30^{o}C, the absence of no-collisional breakup and no-secondary resulted in higher K_{DP} (half an order of magnitude) values than the control run. The absence of all SIP mechanisms results in a higher surface precipitation rate (75%) during the peak rainfall hour, which occurs around 11.30 UTC compared to the control run. In the previous study, Phillips et al. (2017b) have shown that SIP through ice-ice collision breakup can

reduce accumulated surface precipitation in the simulated storm by 20%-40%. They attributed it to the increase in snow particles competing for available liquid and the reduction in their growth by riming. It resulted in smaller ice particles and a reduction in surface precipitation.

7. Results about the influence of PBAPs in the absence of SIP mechanisms

To investigate the role of PBAPs in altering cloud microphysical properties through SIP mechanisms, an additional simulation was performed by eliminating all secondary ice processes from the control run and multiplying the initial loading of all PBAP groups by a factor of 100 (the '*very high-PBAP with no SIP' case*). The results of this simulation are then compared to the no-SIP case as shown in Figure 10.

In the absence of any SIP mechanisms, the 100-fold increase in bioaerosols resulted in minimal effect on ice number concentration. Overall, without SIP the increase in bioaerosol loading by 100-fold resulted in less than a 5% change in ice number concentration. This indicates that the ice produced by various SIP mechanisms does not alter the effect of bioaerosols on-ice number concentration in the simulated clouds. The changes in simulated radar reflectivity due to a 100-fold increase in bioaerosols are negligible (< 0.5%) (Figure 10c). The difference in predicted surface precipitation rate and accumulated precipitation between very high-PBAP with no-secondary and no-secondary cases was lower than 3%.

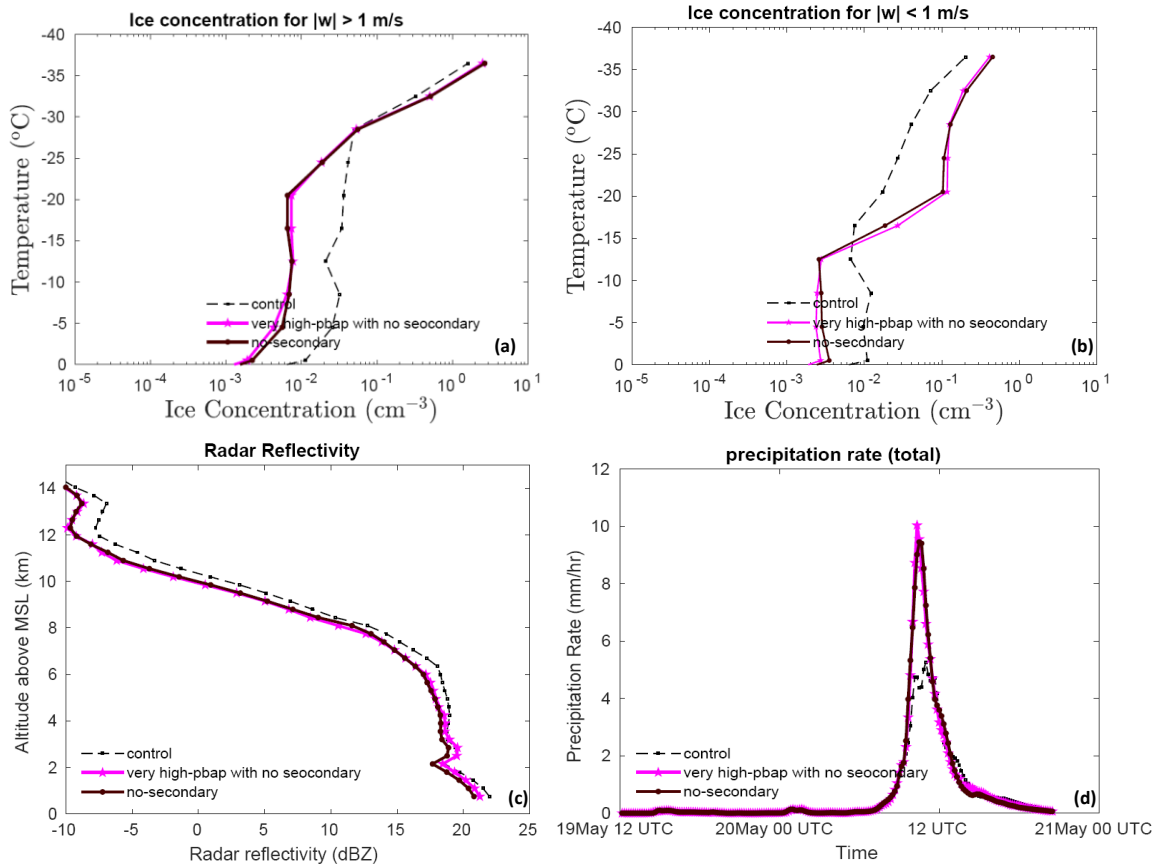

749

750 **Figure 10:** The temperature dependence of ice number concentration for the control, very
751 high-PBAP with no SIP and no-SIP simulations averaged for (a) convective and (b)
752 stratiform regions. The (c) vertical profile of radar reflectivity and the temporal evolution of
753 (d) surface precipitation rate are shown for the entire simulation. All the vertical profiles
754 shown here are averaged for the whole domain. All the vertical profiles shown here are
755 averaged for the whole domain.

756

757 **8. Discussion**

758 Five PBAP groups have been implemented in the mesoscale AC model to predict their ice
759 nucleation activity based on the empirical formulation by PT21. The simulated concentrations
760 of major PBAPs including fungi and bacteria are of the same order of magnitude as results
761 from previous modeling studies (Després et al., 2012; Hoose et al., 2010b). Still, the relative
762 abundance of PBAP groups over the simulated region is unknown due to the lack of
763 measurements. The AC model was run with higher resolution (2 X 2 km) compared to
764 previous studies on a global scale (Hoose et al., 2010b), to investigate the potential impact of

765 variations in PBAP concentration on the properties of simulated squall line events more
766 clearly.

767 Yet the control simulation is not perfectly accurate in all respects. In the stratiform
768 region between -10 and -16^{o}C, the predicted ice number concentration was lower than
769 observed by aircraft by half an order of magnitude and in fair agreement at temperatures
770 warmer than -10^{o}C. This uncertainty factor is similar to the uncertainty in the measurements
771 due to various biases (e.g., Field et al. 2006. Nevertheless, all other simulated cloud
772 microphysical parameters, radar reflectivity, and surface precipitation rate were in acceptable
773 agreement with aircraft and ground-based observations.

774 In the control simulation, the average ice concentration above the -30^{o}C and -18^{o}C
775 levels is dominated by downwelling of homogeneously nucleated ice from above the mixed-
776 phase region in convective and stratiform clouds respectively. Below both levels, SIP
777 prevails. Both processes of ice initiation (homogeneous freezing and SIP) have only weak
778 sensitivity to PBAPs, hence the weakness of the impact on simulated cloud glaciation.

779 Based on the sensitivity experiments, it can be concluded that PBAP INPs have only a
780 limited effect on the average state of the ice phase of the simulated clouds of this mesoscale
781 convective system. Most of the changes in ice number concentration associated with changes
782 in PBAPs are controlled by their effects on homogeneous nucleation and SIPs. The lower
783 dependence of simulated ice number concentration on changes in PBAPs is consistent with
784 the findings of Hummel *et al*. (2018). Based on ensemble simulations of the regional
785 atmospheric model for Europe, they showed that the changes in average ice crystal
786 concentration by biological INPs are very small and are not statistically significant, implying
787 that PBAPs play only a minor role in altering the cloud ice phase. The limited effect of

PBAPs on cloud properties on a global scale has been highlighted in previous studies (Hoose et al., 2010b; Sesartic et al., 2012, 2013; Spracklen and Heald, 2014).

The weakness of the simulated impact from realistic PBAP fluctuations is explicable mostly in terms of the low contribution from biological ice nucleation compared to non-biological INPs to overall ice initiation. In terms of ice nucleation efficiency and onset temperatures, each PBAP group has different ice nucleation properties. Based on vertical profiles of active INPs (Figures 4), the overall contribution of activated INPs from all PBAP groups to the total active INPs was ~1%. At -15^{o}C, temperature, the active INPs from dust and black carbon was one order higher than PBAP INPs. At -30^{o}C, the predicted INPs from dust and black carbon were higher by one and two orders of magnitude, respectively, than PBAP INPs. The dust and black carbon INPs activated at these temperatures can be advected down to the levels where PBAP INPs are most important. Overall, this resulted in low sensitivity of the average ice phase to the changes in bioaerosol loading.

The ice production in the simulated cloud system at levels in the mixed-phase region (0 to -36^{o}C) is largely controlled by various SIP mechanisms of which the most important is the breakup in ice-ice collisions. Some of these processes are active at temperatures warmer than -15^{o}C (e.g., the HM process) where PBAP INP are important and expected to enhance the biological ice nucleation. However, our results showed that the ice production associated with SIP mechanisms is less sensitive to the initial PBAP loading because SIP causes positive feedback of ice multiplication with ice fragments growing to become precipitation-size particles that then fragment again.

In our study, a 100-fold increase in PBAPs leads to a < 4% change in surface precipitation. Using mesoscale model simulations, Phillips et al. (2009) reported a 10% increase in accumulated surface precipitation associated with deep convective clouds due to a

100-fold increase in biological particles. Phillips et al. (2009) also noted an effect (up to 4%) on surface shortwave and TOA longwave radiation flux because of changes in PBAP number concentration. In our study, the changes in PBAP loading caused smaller changes in simulated shortwave and longwave fluxes (< 3%). Sesartic et al. (2012, 2013) showed that including fungi and bacteria in the global climate model leads to minor changes (< 0.5%) in the ice water path, total cloud cover, and total precipitation.

It should be noted that the sensitivity experiments carried out in the current study are limited to the small domain (80 X 80 km domain) representing a limited area of the global ecosystem. Also, the model top was located at 16 km, and it may not represent the whole atmosphere. The results presented here are based on a mesoscale model and may not represent the global impact of PBAPs on clouds.

9. Conclusions

A framework describing the ice nucleation activity of five major groups of PBAPs including fungal spores, bacteria, pollen, viral particles, plant/animal detritus, algae, and their respective fragments was provided by PT21. The ice nucleation activity of these major PBAP groups in the EP was based on samples from the real atmosphere. The present study implements this EP in AC and investigates the role of these five PBAP groups as INPs in deep convective clouds. The high-resolution (2 km horizontally) simulations over a mesoscale 3D domain (80 km wide) using AC elucidate the impact of these PBAP groups on the cloud properties. A series of sensitivity experiments were conducted to test the impact of PBAP groups on cloud properties.

A mid-latitude squall line that occurred on 20 May 2011 during MC3E over the US Southern Great Plains is simulated with the model. The simulated number concentration of ice particles showed good agreement (to within about 50%) with aircraft observations for the convective clouds within the mesoscale system. In the stratiform region between -10 and -16^{o}C, the model predicted ice number concentration was lower than the aircraft observation by half an order of magnitude and in fair agreement at temperatures warmer than -10^{o}C. Various sensitivity experiments were carried out by perturbing the initial PBAP loading and by altering various SIP mechanisms.

Each PBAP group has diverse properties including its shape, size, and abundance in the atmosphere. A small fraction of PBAPs is found to be ice nucleation active and can therefore act as PBAP INPs. The relative contribution of each PBAP within the total PBAPs may vary from one ecosystem to another. In the current study, their relative contribution is based on previous observations from Amazonia and can be considered as the main limitations of this study. However, the simulated number concentrations of major PBAPs including fungi, and bacteria look reasonable and are close to their typical abundance in the atmosphere.

Any perturbation in the PBAP concentration by factors upto 1000 assumed in the current study (resulted in maximum changes in ice number concentration by < 6% convective region and by < 40% in the stratiform region with respect to the control run. The simulations showed that simulated ice particle number concentration is much higher than the number concentrations of PBAP INPs. Even at temperatures warmer than -15^{o}C, where PBAP INPs are thought to be the most important INP, ice crystals originated from primary heterogeneous nucleation of dust and black carbon from higher levels of the cloud frequently perturb the lower levels due to sedimentation. The major ice formation comes from SIP mechanisms and

homogeneous nucleation, both are less sensitive to the changes in PBAPs. Therefore, PBAP INPs do not show a significant impact on the average ice phase of the simulated storm.

PBAPs have minimal effect on the warm microphysical properties of simulated clouds. The effect on liquid water content and cloud droplet number concentration was lower than 10% in both convective and stratiform regions. Since both ice and warm microphysical processes are less sensitive to PBAPs, surface precipitation is not affected significantly by changes in PBAPs. A 100-fold increase in all PBAPs resulted in less than a 5% change in surface precipitation.

Code and data availability: Data and the code for the empirical formulation of PBAPs are available on request by contacting the corresponding author.

Competing interests: The authors declare no conflict of interest

Author Contributions: VJTP designed and monitored this study. SP conducted model simulation, most of the data analysis, and wrote the initial manuscript. All authors contributed to the scientific discussion and model development.

Financial support: This work was completed for a sub-award (award number: 2019-26-03) to VTJP from a US Department of Energy (DoE) direct grant to the Ryzhkov at the University of Oklahoma (award number: DE-SC0018967). The first author was also supported by a past award from the Swedish Research Council ('VR'), which concerns modeling bio-aerosol effects on glaciated clouds (2015-05104) and Sweden's Innovation Agency (Vinnova; 2020-03406). Other co-authors were supported by a current award from the Swedish Research Council for Sustainable Development (FORMAS; award number 2018-01795) and the US Department of Energy Atmospheric Sciences Research Program (award number: DE-SC0018932).

References:

Blyth, A. M., Latham, J.: Development of ice and precipitation in New Mexican summertime cumulus clouds. Q. J. R. Meteorol. Soc. 119:91–120, 1993.

Baumgardner, D., Abel, S. J., Axisa, D., Cotton, R., Crosier, J., Field, P., Gurganus, C., Heymsfield, A., Korolev, A., Krämer, M., Lawson, P., McFarquhar, G., Ulanowski, Z., & Um, J.: Cloud Ice Properties: In Situ Measurement Challenges, *Meteorological Monographs*, *58*, 9.1-9.23, 2017.

Bowers, R. M., Lauber, C. L., Wiedinmyer, C., Hamady, M., Hallar, A. .G., Fall, R., Knight, R., Fierer, N.: Characterization of airborne microbial communities at a high-elevation site and their potential to act as atmospheric ice nuclei. Appl Environ Microbiol, Aug;75(15):5121-30. doi: 10.1128/AEM.00447-09, 2009.

Bauer, H., Kasper-Giebl, A., Loflund, M., Giebl, H., Hitzenberger, R., Zibuschka, F., and Puxbaum, H.: The contribution of bacteria and fungal spores to the organic carbon content of cloud water, precipitation and aerosols, Atmos. Res., 64, 109–119, 2002.

Burrows, S. M., Elbert, W., Lawrence, M. G., and Pöschl, U.: Bacteria in the global atmosphere – Part 1: Review and synthesis of literature data for different ecosystems, Atmos. Chem. Phys., 9, 9263–9280, 2009.

Carlin, J. T., Reeves, H. D., & Ryzhkov, A. V: Polarimetric Observations and Simulations of Sublimating Snow: Implications for Nowcasting, Journal of Applied Meteorology and Climatology, 60(8), 1035-1054, 2021.

Chen, Q., Yin, Y., Jiang, H., Chu, Z., Xue, L., Shi, R., et al. : The roles of mineral dust as cloud condensation nuclei and ice nuclei during the evolution of a hail storm. *Journal of Geophysical Research: Atmospheres*, 2019; 124: 14262– 14284, 2019.

Chin, M., Rood, R. B., Lin, S. J., Müller, J. F., and Thompson, A. M.: Atmospheric sulfur cycle simulated in the global model GOCART: Model description and global properties. *Journal of Geophysical Research Atmospheres*, **105**, 24671–24687, https://doi.org/10.1029/2000JD900384, 2000.

Crawford, I., Bower, K. N., Choularton, T. W., Dearden, C., Crosier, J., Westbrook, C., Capes, G., Coe, H., Connolly, P. J., Dorsey, J. R., Gallagher, M. W., Williams, P., Trembath, J., Cui, Z., and Blyth, A.: Ice formation and development in aged, wintertime cumulus over the UK: observations and modelling, Atmos. Chem. Phys., 12, 4963–4985, https://doi.org/10.5194/acp-12-4963-2012, 2012.

Cui, Z., and Carslaw, K. S.,: Enhanced vertical transport efficiency of aerosol in convective clouds due to increases in tropospheric aerosol abundance, J. Geophys. Res., 111, D15212, doi:10.1029/2005JD006781, 2006.

Deshmukh, A., Phillips, V. J. T. P, Bansemer A., Patade, S., and Waman, D.: New Empirical Formulation for the Sublimational Breakup of Graupel and Dendritic Snow, DOI: https://doi.org/10.1175/JAS-D-20-0275.1, 2021.

928 Després, V. R., and Coauthors: Primary biological aerosol particles in the atmosphere: A
929 review. *Tellus, Series B: Chemical and Physical Meteorology*, **64**,
930 https://doi.org/10.3402/tellusb.v64i0.15598, 2012

931 DeMott P. J., Prenni A. J., Liu, X., Kreidenweis, S. M., Petters, M. D., Twohy, C.H., *et al.*
932 Predicting global atmospheric ice nuclei distributions and their impacts on climate Proc.
933 Natl. Acad. Sci. U. S. A., 107, pp. 11217-11222, 2010.

934 DeMott, P. J. and Prenni, A. J.: New Directions: Need for defining the numbers and sources
935 of biological aerosols acting as ice nuclei, Atmos. Environ., 44, 1944–1945, 2010.

936 Despr´es, V.R., Huffman, J. A., Burrows, S. M., Hoose, C., Safatov, A .S., Buryak, G.,
937 Fr¨ohlich-Nowoisky, J., Elbert, W., Andreae, M. O., P¨oschl, U.: Primary
938 biological aerosol particles in the atmosphere: a review. Tellus B Chem. Phy.
939 Meteorol. 64 (1), 15598, 2012.

940 Dong, X., Mace and G. G.: Arctic stratus cloud properties and radiative forcing derived from
941 ground-based data collected at Barrow, Alaska. *J. Climate*, **16**, 445–461,
942 doi:10.1175/1520-0442(2003)016<0445:ASCPAR>2.0.CO;2, 2003.

943 Han, B., Fan, J., Varble, A., Morrison, H., Williams, C. R., Chen, B., et al.: Cloud-resolving
944 model intercomparison of an MC3E squall line case: Part II. Stratiform precipitation
945 properties. *Journal of Geophysical Research: Atmospheres*, 124, 1090– 1117, 2019.

946 Fan, J., Liu, Y-C, Xu, K.M., North, K., Collis, S., Dong, X., Zhang, G.J., Chen, Q., Kollias,
947 P., and Ghan, S.J.: Improving representation of convective transport for scale-aware
948 parameterization: 1. Convection and cloud properties simulated with spectral bin and
949 bulk microphysics. J. Geophys. Res. Atmos., 120, 3485– 3509. doi:
950 10.1002/2014JD022142, 2015.

951 Fan J., Comstock J.M., Ovchinnikov M.: The cloud condensation nuclei and ice nuclei
952 effects on tropical anvil characteristics and water vapor of the tropical tropopause layer
953 Environ. Res. Lett., 5 Article 044005, 10.1088/1748-9326/5/4/044005, 2010.

954 Fan, J., Han, B., Varble, A., Morrison, H., North, K., Kollias, P., Chen, B., Dong, X.,
955 Giangrande, S., Khain, A., Lin, Y., Mansell, E., Milbrandt, J. A., Stenz, R., Thompson,
956 G., Wang Y: Cloud-resolving model intercomparison of an MC3E squall line case: Part
957 I—Convective updrafts, *J. Geophys. Res. Atmos.*, 122, 9351– 9378, 2017.

958 Field, P. R., and Heymsfield A. J: Importance of snow to global precipitation, Geo-phys.
959 Res. Lett., 42, 9512–9520,doi:10.1002/2015GL065497, 2015.

960 Field, P. R., Heymsfield, A. J., & Bansemer, A.: Shattering and Particle Interarrival Times
961 Measured by Optical Array Probes in Ice Clouds, Journal of Atmospheric and Oceanic
962 Technology, 23(10), 1357-1371, 2006.

963 Fridlind, A. M., and Coauthors: Derivation of aerosol profiles for MC3E convection studies
964 and use in simulations of the 20 May squall line case. *Atmospheric Chemistry and*
965 *Physics*, **17**, 5947–5972, https://doi.org/10.5194/acp-17-5947-2017, 2017.

966 Fr¨ohlich-Nowoisky, J., Kampf, C. J., Weber, B., Huffman, J.A., P¨ohlker, C., Andreae, M.
967 O., Lang-Yona, N., Burrows, S.M., Gunthe, S.S., Elbert, W., Su, H., Hoor, P.,
968 Thines, E., Hoffmann, T., Despr´es, V.R., P¨oschl, U.: Bioaerosols in the Earth
969 system: climate, health, and ecosystem interactions. Atmos. Res. 182, 346–376, 2016.

970 Garcia, E., Hill, T. C. J., Prenni, A. J., DeMott, P. J., Franc, G. D., and Kreidenweis, S. M.:
971 Biogenic ice nuclei in boundary layer air over two US high plains agricultural regions.
972 *Journal of Geophysical Research Atmospheres*, **117**, 1–12,
973 https://doi.org/10.1029/2012JD018343, 2012.

974 Giangrande, S. E., Collis, S., Theisen, A. K., and Tokay, A.,: Precipitation estimation from
975 the ARM distributed radar network during the MC3E campaign. *Journal of Applied*
976 *Meteorology and Climatology*, **53**, 2130–2147, https://doi.org/10.1175/JAMC-D-13-
977 0321.1, 2014.

978 Grützun, V., Knoth, O., and Simmel, M.,: Simulation of the influence of aerosol particle
979 characteristics on clouds and precipitation with LM-SPECS: Model description and first
980 results. *Atmospheric Research*, **90**, 233–242,
981 https://doi.org/10.1016/j.atmosres.2008.03.002, 2008.

982 Hallett, J., and Mossop S. C.: Production of secondary ice particles during the riming process.
983 Nature, 249, 26–28, https://doi.org/10.1038/249026a0, 1974.

984 Heymsfield, A. J., Schmitt, C., Chen, C., Bansemer, A., Gettelman, A., Field, P. R., & Liu, C.
985 : Contributions of the Liquid and Ice Phases to Global Surface Precipitation:
986 Observations and Global Climate Modeling, Journal of the Atmospheric Sciences, 77(8),
987 2629-2648, 2020.

988 Hoose, C., and Möhler, O.: Heterogeneous ice nucleation on atmospheric aerosols: A review
989 of results from laboratory experiments. *Atmospheric Chemistry and Physics*, **12**, 9817–
990 9854, https://doi.org/10.5194/acp-12-9817-2012, 2012.

991 Hoose, C., Kristjánsson J. E., and Burrows S. M.: How important is biological ice nucleation
992 in clouds on a global scale? *Environmental Research Letters*, **5**,
993 https://doi.org/10.1088/1748-9326/5/2/024009, 2010.

994 Hoose, C., Kristjánsson, J. E., Chen, J. P., and Hazra, A.: A Classical-Theory-Based
995 Parameterization of Heterogeneous Ice Nucleation by Mineral Dust, Soot, and
996 Biological Particles in a Global Climate Model, J. Atmos. Sci., 67, 2483–
997 2503, https://doi.org/10.1175/2010jas3425.1, 2010b.

998 Huang, S., Wei, H., Chen, J., Wu, Z., Zhang, D., Fu P.: Overview of biological ice
999 nucleating particles in the atmosphere, Environment International, Volume 146,106197,
1000 2021.

Huffman, J. A., and Coauthors: High concentrations of biological aerosol particles and ice nuclei during and after rain. *Atmospheric Chemistry and Physics*, **13**, 6151–6164, https://doi.org/10.5194/acp-13-6151-2013, 2013.

Hummel, M., Hoose, C., Pummer, B., Schaupp, C., Fröhlich-Nowoisky, J., and Möhler, O.: Simulating the influence of primary biological aerosol particles on clouds by heterogeneous ice nucleation. *Atmospheric Chemistry and Physics*, **18**, 15437–15450, https://doi.org/10.5194/acp-18-15437-2018, 2018.

Jensen, M. P., and Coauthors: The midlatitude continental convective clouds experiment (MC3E). *Bulletin of the American Meteorological Society*, **97**, 1667–1686, https://doi.org/10.1175/BAMS-D-14-00228.1, 2016.

Jaenicke, R.: Abundance of cellular material and proteins in the atmospheric. Science 308, 73, 2005.

Kanji, Z. A., Ladino, L. A., Wex, H., Boose, Y., Burkert-Kohn, M., Cziczo, D. J., & Krämer, M.: Overview of Ice Nucleating Particles, Meteorological Monographs, 58, 1.1-1.33, 2017.

Korolev, A. V., Kuznetsov, S. V., Makarov, Y. E., & Novikov, V. S: Evaluation of Measurements of Particle Size and Sample Area from Optical Array Probes, Journal of Atmospheric and Oceanic Technology, 8(4), 514-522. 1991.

Korolev, A., McFarquhar, G., Field, P. R., Franklin, C., Lawson, P., Wang, Z., Williams, E., Abel, S. J., Axisa, D., Borrmann, S., Crosier, J., Fugal, J., Krämer, M., Lohmann, U., Schlenczek, O., Schnaiter, M., & Wendisch, M.: Mixed-Phase Clouds: Progress and Challenges, *Meteorological Monographs*, *58*, 5.1-5.50, 2017.

Korolev, A. and Leisner, T.: Review of experimental studies of secondary ice production, Atmos. Chem. Phys., 20, 11767–11797, https://doi.org/10.5194/acp-20-11767-2020, 2020.

Korolev, A., Heckman, I., Wolde, M., Ackerman, A. S., Fridlind, A. M., Ladino, L. A., Lawson, R. P., Milbrandt, J., and Williams, E.: A new look at the environmental conditions favorable to secondary ice production, Atmos. Chem. Phys., 20, 1391–1429, https://doi.org/10.5194/acp-20-1391-2020, 2020.

Kumjian, M. R, and Lombardo, K. A: Insights into the evolving microphysical and kinematic structure of northeastern U.S. winter storms from dual-polarization Doppler radar. Mon. Wea. Rev., 145, 1033–1061, https://doi.org/10.1175/MWR-D-15-0451.1, 2017.

Knopf, D. A., Alpert, P.A., Wang, B., Aller, J.Y.: Stimulation of ice nucleation by marine diatoms. Nat. Geosci. 4, 88–90. https://doi.org/10.1038/ngeo1037, 2011.

Lawson, R. P., Woods, S. and Morrison, H.: The microphysics of ice and precipitation 1195 development in tropical cumulus clouds, J. Atmos. Sci., 72(6), 2429–2445, 1196 doi:10.1175/JAS-D-14-0274.1, 2015.

Levin, Z., Yankofsky, S., Pardes, D. and Magal, N.: J. Clim. Appl. Meteorol. 26 1188–97, 1987.

Matus, A. V. and L'Ecuyer, T. S.: The role of cloud phase in Earth's radiation budget, J. Geophys. Res. Atmos., 122, 2559– 2578, doi:10.1002/2016JD025951, 2017.

Malm, W. C., Sisler, J. F., Huffman, D., Eldred, R. A., and Cahill T. A.: Spatial and seasonal trends in particle concentration and optical extinction in the United States, J. Geophys. Res., 99, 1347-1370, 1994.

Matthias-Maser, S., Bogs, B., Jaenicke, R.: The size distribution of primary biological aerosol particles in cloud water on the mountain Kleiner Feldberg/Taunus (FRG), Atmospheric Research, Volume 54, Issue 1, Pages 1-13, 2000.

Mattias-Maser, S., Brinkmann, J., Schneider, W.: The size distribution of marine atmospheric aerosol with regard to primary biological aerosol particles over the South Atlantic Ocean. Atmospheric Environment 33, 3569–3575, 1999.

Mattias-Maser, S., Jaenicke, R.: The size distribution of primary biological aerosol particles with radii > 0.2 mm in an urban/rural influenced region. Atmospheric Research 39, 279–286, 1995.

Mülmenstädt, J., Sourdeval, O., Delanoë, J., and Quaas, J.: Frequency of occurrence of rain from liquid-, mixed-, and ice-phase clouds derived from A-Train satellite retrievals, Geophys. Res. Lett., 42, 6502– 6509, 2015.

Möhler, O., and Coauthors: *Heterogeneous ice nucleation activity of bacteria: new laboratory experiments at simulated cloud conditions*. 1425–1435 pp. www.biogeosciences.net/5/1425/2008/, 2008.

Moisseev, D. N., Lautaportti, S., Tyynela, J., and Lim, S. (2015), Dual-polarization radar signatures in snowstorms: Role of snowflake aggregation, *J. Geophys. Res. Atmos.*, 120, 12644– 12655, doi:10.1002/2015JD023884.

Morris, C. E., Conen F., Huffman, A. J., Phillips, V. J. T. P., Pöschl, U., and Sands, D. C.: Bioprecipitation: A feedback cycle linking Earth history, ecosystem dynamics and land use through biological ice nucleators in the atmosphere. *Global Change Biology*, **20**, 341–351, https://doi.org/10.1111/gcb.12447, 2014,

Murray, B. J., O'Sullivan D., Atkinson J. D., and Webb M. E.,: Ice nucleation by particles immersed in supercooled cloud droplets. Chem. Soc. Rev., 41, 6519–6554, https://doi.org/ 10.1039/c2cs35200a., 2012.

Patade, S., Phillips, V. T. J., Amato, P., Bingemer, H. G., Burrows, S. M., DeMott, P. J., Goncalves, F. L. T., Knopf, D. A., Morris, C. E., Alwmark, C., Artaxo, P., Pöhlker, C., Schrod, J., & Weber, B.: Empirical Formulation for Multiple Groups of Primary Biological Ice Nucleating Particles from Field Observations over Amazonia, Journal of the Atmospheric Sciences, 78(7), 2195-2220, 2021.

Phillips, V. T. J., Donner, L. J., and Garner, S.: Nucleation processes in deep convection simulated by a cloud-system resolving model with double-moment bulk microphysics, J. Atmos. Sci., 64, 738– 761, 2007.

Phillips, V. T. J., DeMott, P. J., & Andronache, C.: An Empirical Parameterization of Heterogeneous Ice Nucleation for Multiple Chemical Species of Aerosol, Journal of the Atmospheric Sciences, 65(9), 2757-2783, 2008.

Phillips, V. T. J., and Coauthors: Potential impacts from biological aerosols on ensembles of continental clouds simulated numerically. *Biogeosciences*, **6**, 987–1014, https://doi.org/10.5194/bg-6-987-2009. , 2009

Phillips, V. T. J., Yano, J., Formenton, M., Ilotoviz, E., Kanawade, V., Kudzotsa, I., Sun, J., Bansemer, A., Detwiler, A. G., Khain, A., & Tessendorf, S. A.: Ice Multiplication by Breakup in Ice–Ice Collisions. Part II: Numerical Simulations, Journal of the Atmospheric Sciences, 74(9), 2789-2811, 2017b.

Phillips, V. T. J., Formenton, M., Kanawade, V. P., Karlsson, L. R., Patade, S., Sun, J., Barthe, C., Pinty, J., Detwiler, A. G., Lyu, W., & Tessendorf, S. A.: Multiple Environmental Influences on the Lightning of Cold-Based Continental Cumulonimbus Clouds. Part I: Description and Validation of Model, Journal of the Atmospheric Sciences, 77(12), 3999-4024, 2020.

Phillips, V. T. J., Yano, J. I., and Khain, A.,: Ice multiplication by breakup in ice-ice collisions. Part I: Theoretical formulation. *Journal of the Atmospheric Sciences*, **74**, 1705–1719, https://doi.org/10.1175/JAS-D-16-0224.1, 2017a.

Phillips, V. T. J., Demott, P. J., Andronache, C., Pratt, K. A., Prather, K. A., Subramanian, R., and Twohy, C.: Improvements to an empirical parameterization of heterogeneous ice nucleation and its comparison with observations. *Journal of the Atmospheric Sciences*, **70**, 378–409, https://doi.org/10.1175/JAS-D-12-080.1, 2013.

Phillips, V. T. J., Patade, S: Multiple Environmental Influences on the Lightning of Cold-based Continental Convection. Part II: Sensitivity Tests for its Charge Structure and Land-Ocean Contrast. *Journal of the Atmospheric Sciences*, https://doi.org/10.1175/JAS-D-20-0234.1., 2021.

Phillips, V. T. J., Patade, S., Gutierrez, J., and Bansemer, A.: Secondary ice production by fragmentation of freezing drops: Formulation and theory. *Journal of the Atmospheric Sciences*, **75**, 3031–3070, https://doi.org/10.1175/JAS-D-17-0190.1, 2018.

Prenni, A. J., and Coauthors: The impact of rain on ice nuclei populations at a forested site in Colorado. *Geophysical Research Letters*, **40**, 227–231, https://doi.org/10.1029/2012GL053953, 2013.

Pörtner, H. O., et al.: Summary for policymakers. In: Climate change 2022: Impact, adaptation, and vulnerability: Summary for policy makers: Working group II Contribution to the sixth assessment report of the Intergovernmental Panel on Climate Change, 2022.

Ryzhkov, A., Pinsky, M., Pokrovsky, A., & Khain, A.: Polarimetric Radar Observation Operator for a Cloud Model with Spectral Microphysics, Journal of Applied Meteorology and Climatology, 50(4), 873-894, 2011.

Sahyoun, M., Wex, H., Gosewinkel, U., Šantl-Temkiv, T., Nielsen, N. W., Finster, K., Sørensen, J. H., Stratmann, F., and Korsholm, U. S.: On the usage of classical nucleation

theory in quantification of the impact of bacterial INP on weather and climate, Atmos. Environ., 139, 230–240, https://doi.org/10.1016/j.atmosenv.2016.05.034, 2016.

Sesartic, A., Lohmann, U., and Storelvmo T: Bacteria in the ECHAM5-HAM global climate model. *Atmospheric Chemistry and Physics*, **12**, 8645–8661, https://doi.org/10.5194/acp-12-8645-2012, 2012.

Sesartic, A., Lohmann, U., and Storelvmo, T.: Modelling the impact of fungal spore ice nuclei on clouds and precipitation. *Environmental Research Letters*, **8**, https://doi.org/10.1088/1748-9326/8/1/014029, 2013.

Sinclair, V. A., Moisseev, D., and von Lerber, A. (2016), How dual-polarization radar observations can be used to verify model representation of secondary ice, J. Geophys. Res. Atmos., 121, 10,954– 10,970, doi:10.1002/2016JD025381.

Sotiropoulou, G., Ickes, L., Nenes, A. and Ekman, A.: Ice multiplication from ice–ice collisions in the high Arctic,: sensitivity to ice habit, rimed fraction, ice type and uncertainties in the numerical description of the process, Atmos. Chem. Phys., 21, 9741–9760, 1313 doi:10.5194/acp-21-9741-2021, 2021b

Sotiropoulou, G., Vignon, E., Young, G., Morrison, H., O'Shea, S. J., Lachlan-Cope, T., Berne, A. and Nenes, A.: Secondary ice production in summer clouds over the Antarctic coast: 1308 An underappreciated process in atmospheric models, Atmos. Chem. Phys., 21(2), 755– 1309 771, doi:10.5194/acp-21-755-2021, 2021a.

Spracklen, D. V., and Heald, C. L: The contribution of fungal spores and bacteria to regional and global aerosol number and ice nucleation immersion freezing rates. *Atmospheric Chemistry and Physics*, **14**, 9051–9059, https://doi.org/10.5194/acp-14-9051-2014, 2014

Szyrmer, W., Zawadzki, I.: Biogenic and anthropogenic sources of ice-forming nuclei: A review. Bull. Am. Meteorol. Soc. 78, 209–228, 1997.

Tsushima, Y., Emori S., Ogura T. et al.: Importance of the mixed-phase cloud distribution in the control climate for assessing the response of clouds to carbon dioxide increase: a multi-model study. Clim Dyn 27, 113–126, 2006.

Wilson, T., and Coauthors: A marine biogenic source of atmospheric ice-nucleating particles. Nature, 525, 234–238, https://doi.org/10.1038/nature14986, 2015.

Xie, S., Y. Zhang, S. E. Giangrande, M. P. Jensen, R. McCoy, and M. Zhang: Interactions between cumulus convection and its environment as revealed by the MC3E sounding array. *Journal of Geophysical Research*, **119**, 11,784-11,808, https://doi.org/10.1002/2014JD022011, 2014.

Zhao, X., & Liu, X.: Global importance of secondary ice production. *Geophysical Research Letters*, 48, e2021GL092581. https://doi.org/10.1029/2021GL092581, 2021.

Zuidema, P., E. R. Westwater, C. Fairall, and Hazen, D.: Ship-based liquid water path estimates in marine stratocumulus. *J. Geophys. Res.*, **110**, D20206, doi:10.1029/2005JD005833, 2005.